Nonlinear Dyn
https://doi.org/10.1007/s11071-020-05689-1

ORIGINAL PAPER

Chaos, border collisions and stylized empirical facts in an asset pricing model with heterogeneous agents

Mikhail Anufriev · Laura Gardini · Davide Radi

Received: 14 January 2020 / Accepted: 7 May 2020

Abstract An asset pricing model with chartists, fundamentalists and trend followers is considered. A market maker adjusts the asset price in the direction of the excess demand at the end of each trading session. An exogenously given fundamental price discriminates between a bull market and a bear market. The buying and selling orders of traders change moving from a bull market to a bear market. Their asymmetric propensity to trade leads to a discontinuity in the model, with its deterministic skeleton given by a two-dimensional piecewise linear dynamical system in discrete time. Multiple attractors, such as a stable fixed point and one or more attracting cycles or cycles and chaotic attractors, appear through border collision bifurcations. The multi-stability regions are underlined by means of two-dimensional bifurcation diagrams, where the border collision bifurcation curves are detected in analytic form at least for basic cycles with symbolic sequences LR^n and RL^n. A statistical analysis of the simulated time series of the asset returns, generated by perturbing the deterministic dynamics with a random walk process, indicates that this is one of the simplest asset pricing models which are able to replicate stylized empirical facts, such as excess volatility, fat tails and volatility clustering.

Keywords Piecewise linear asset pricing model · Heterogeneous traders · Chaos and border collision bifurcations · Stylized empirical facts of asset returns

M. Anufriev (✉)
Department of Economics, University of Technology Sydney, Sydney, Australia
e-mail: Mikhail.Anufriev@uts.edu.au

L. Gardini
Department of Economics, Society and Politics, University of Urbino, Urbino, Italy
e-mail: laura.gardini@uniurb.it

D. Radi
Department of Economics and Management, University of Pisa, Pisa, Italy
e-mail: davide.radi@unipi.it; davide.radi@vsb.cz

D. Radi
Department of Finance, VŠB–Technical University of Ostrava, Ostrava, Czech Republic

1 Introduction

The financial literature is devoted to investigate the mechanisms that determine prices and returns of financial assets. The mainstream modeling approach starting from the hypothesis that traders are rational and have perfect foresight (or rational expectations) leads to the so-called *efficient market hypothesis*. According to such approach, the price of an asset follows a random walk process and is the best prediction for its 'fundamental value,' given by the discounted stream of dividends. An alternative approach is represented by the financial market models with heterogeneous traders, as well as their less tractable counter-part, agent-based financial market models. These models relax the hypotheses of full rationality and perfect foresight in expectations and instead are constructed on the basis of simple behavioral rules chosen from a jun-

Published online: 23 May 2020

gle of possible alternatives. The success of these *models of bounded rationality* depends on their ability to replicate 'stylized facts' of stock markets that are not contemplated or replicable by the mainstream models. Regarding asset returns, for example, a common set of stylized empirical facts includes fat tails (i.e., the empirical distribution of the returns has tails fatter than the ones of the normal distribution), extreme fluctuations (i.e., fluctuations that exceed those generated by a random walk fundamental process), linear and nonlinear dependence of returns in time, volatility clustering (i.e., periods of high volatility that persist over time and are alternated to periods of low volatility), see, e.g., Lux and Mar [33], Cont [12], and Lux and Ausloos [32].

The agent-based approach offers wide degrees of freedom regarding the modeling choices, and the heterogeneity may reflect both diverse intrinsic attitudes of traders, such as speculative trading behaviors versus prudent trading behaviors, and diverse expectations on the future prices of assets and their riskiness. The parsimonious versions of these models have a deterministic skeleton which is represented by a low-dimensional dynamical system. One of the first baseline versions of these models is the one proposed in [13], where three types of traders coexist. Traders of the first type (*chartists*) have the propensity to speculate: they place buying orders in a bull market and selling orders in a bear market. Traders of the second type (*fundamentalists*) are not inclined to speculate: they place buying orders in a bear market and selling orders in a bull market. Finally, a third type of trader (*market maker*) has the power to adjust the market price of the asset in the direction of the excess of total asset demand. A founding assumption is the existence of a so-called fundamental price, which represents the price of the asset under the efficient market hypothesis, allowing to distinguish between bull and bear markets. A generalization of this model that accounts for a propensity to trade by chartists and fundamentalists that changes according to the type of market, bull or bear, is proposed in Tramontana et al. [47]. It is a simple one-dimensional piecewise linear financial market model with heterogeneous interacting traders, where the set of traders includes two types of chartists, two types of fundamentalists and a market maker.

In this paper, we extend the model in Tramontana et al. [47] by introducing another type of trader, the trend follower, which places buying/selling orders in an upward/downward price trend. The magnitude of the buying/selling order that follows a positive/negative price trend may differ from a bull market to a bear market. The introduction of this trader increases the dimension of the deterministic skeleton of the model, obtaining a two-dimensional piecewise linear map. A peculiarity of this generalized version of the model is the coexistence of several attractors, such as a stable equilibrium that coexists with a stable cycle, or multiple period cycles that are stable and may coexist with chaotic attractors. This feature of multi stability with cycles is essential for the stochastic version (where the fundamental price follows a random walk process) to be able to replicate stylized empirical facts such as volatility clustering. Since coexisting stable attractors cannot be obtained in the one-dimensional version of the model, see Tramontana et al. [47], the current paper adds to the financial literature by offering an asset pricing model that is able to replicate the stylized facts of asset returns.

The set of parsimonious asset pricing models with heterogeneous agents able to replicate stylized facts of the empirical distribution of the returns is not a singleton. The set includes the model proposed in He and Li [26], which is based on the assumption that traders are mean-variance maximizers (instead of considering simple trading behavioral attitudes) and use heterogeneous rules to forecast future prices and volatility. A similar micro-founded asset pricing model with chartists and fundamentalists is proposed in Brock and Hommes [10], see also the survey in Chiarella et al. [11]. Instead of considering a market maker, in Brock and Hommes [10] the asset price is determined by equating demand and supply. Moreover, the populations of chartists and fundamentalists vary according to an evolutionary mechanism, see Hofbauer and Sigmund [27], that prizes the trading strategies that performed better in the past. The full-fledged stochastic and generalized versions of this model are able to replicate most of the stylized facts of the distribution of the returns mentioned above, see, e.g., Gaunersdorfer et al. [23] and Blaurock et al. [7]. The generalization to the multi-asset setup is also relevant, see, e.g., Dieci et al. [16]. The deterministic skeleton of these asset pricing models cannot be reduced, however, to a piecewise linear configuration. Therefore, our modeling setup has the advantage of being simpler to investigate and to employ.

Shifting the attention to the mathematical aspects, the current contribution adds also to the literature on

piecewise smooth (PWS) systems, which can be classified in continuous and discontinuous systems. Focusing on the bifurcations that characterize such systems, we recap that an invariant set of a smooth dynamical system may undergo the so-called smooth bifurcations, while in a PWS system the dynamics is usually affected by the interplay of smooth bifurcations and border collision bifurcations (BCBs). A border collision takes place whenever an invariant set collides with the border at which the map changes definition, and this may occur in a continuous or discontinuous way. Moreover, when the colliding set is a periodic orbit, the effect of the collision is clearly independent of the eigenvalues of the Jacobian matrix. This marks a first relevant difference between smooth bifurcations and BCBs.

The possibility to have border collision bifurcations impacts also the way a system converges to a chaotic regime. It is well known that the dynamics of smooth systems may go from a regular to a complex behavior via a sequence of bifurcations, such as *Feigenbaum cascades of period doubling bifurcations*, *Neimark–Sacker bifurcations followed by frequency locking*, *homoclinic bifurcations*. A quite different behavior can be observed in PWS systems, where BCBs may occur, leading to a sharp transition of the dynamics from non-chaotic to chaotic regimes, as first evidenced in Nusse and Yorke [36] and Nusse and Yorke [37]. In particular, in piecewise linear (PWL) systems mainly BCBs and contact bifurcations occur. These features make PWS systems suitable to mimic the time series, specifically the sudden changes, of prices and returns in the financial markets.

In addition to economics and finance, PWS systems have a wide spectrum of applications in engineering and other fields. This raised a great interest among scholars, who have extensively studied PWS systems in the last two decades, see, e.g., di Bernardo et al. [15], Zhusubaliyev and Mosekilde [50]. Many works are devoted to PWS, and in particular to the subset of piecewise linear (PWL), one-dimensional maps (see [2,4,18,22], and references therein), where the so-called *period adding* and *period incrementing* bifurcation structures, occurring in the parameter space, are described. The bifurcations in two-dimensional continuous dynamical systems have also been investigated, see, among others, Simpson [40], Simpson [41], Sushko and Gardini [45], Sushko and Gardini [46]. Differently, the description of the bifurcations occurring in two-dimensional discontinuous systems is still not well developed. A class of PWL two-dimensional maps has been considered in Mira et al. [35], Rakshit et al. [38], Kollár et al. [29], Dutta et al. [19], where some preliminary considerations can be found. The investigation of the PWL two-dimensional system considered in this paper underlines a relevant feature of its bifurcation structures. In fact, one peculiarity of one-dimensional piecewise linear, discontinuous, maps is the occurrence of period adding and period incrementing bifurcation structures mentioned above. Some authors have evidenced that it is possible to observe similar structures also in two-dimensional piecewise linear, discontinuous, maps, see Mira [34] and Simpson [43]. The current investigation increases the knowledge on the bifurcation structures of PWL two-dimensional systems by underlining a possible overlapping of periodicity regions in the parameters space, as well as attracting cycles coexisting with chaotic attractors, which cannot occur in the one-dimensional version.

This work is related to the recent applications modeling the dynamics of financial markets and represented by two-dimensional discontinuous systems that appeared in different journals, for example Lu et al. [30], Gu [24], Gu [25], Brianzoni and Campisi [9]. In comparison with these contributions, we propose a model that is more parsimonious as it involves only one discontinuity line. Moreover, in addition to the technical investigation of the deterministic dynamics, we provide a statistical description of the full-fledged stochastic version of the model and we discuss its ability to replicate the main stylized empirical facts.

The road map of the paper is as follows: Sect. 2 introduces the asset pricing model. Section 3 investigates the dynamics of the deterministic skeleton of the model by focusing on the border collision bifurcations that involve fixed points and limit cycles. Specifically, the border collision bifurcation curves for basic cycles of symbolic sequences LR^n and RL^n are detected. Section 4 shows regimes with chaotic attractors in the deterministic setting, which are also robust and may coexist with attracting cycles. The role of the fixed points (real or virtual) is evidenced, as well as one of the borders of the basins of attraction related to the discontinuity line. Section 5 investigates how different configurations of the deterministic structure of the dynamics impact on the distribution of the returns obtained by simulating the stochastic version of the model. Section 6 concludes.

2 The setup of a discontinuous model of a financial market

The setup of a simple financial market model is presented in this section. This model describes a market in which traders can be classified in six types of agents according to their trading propensity. In particular, the market is populated by two types of fundamental traders (fundamentalists) who believe in mean reversion, by two types of technical traders (chartists) who bet on the persistence of bull and bear markets and by a trend follower who believe in the persistence of the trend of prices observed. Moreover, the market is regulated by a market maker who adjusts prices according to excess demand. Technical traders and fundamental traders are classified in two groups according to the trading rules they used: some of them use standard (conventional) linear trading rules while others prefer to trade a constant amount of assets. Traders may also have trading propensities that change when the market changes from bull to bear and vice versa. In the following, the formal definition of the model is derived, the deterministic skeleton of which is described by a simple two-dimensional discontinuous map.

In the current setup, the log fundamental value of the stock market, that is, F_t, follows a random walk:

$$F_{t+1} = F_t + \epsilon_{t+1} \tag{1}$$

where ϵ_{t+1} is a random variable that represents the logarithmic fundamental shocks that are normally distributed with constant standard deviation σ_F. To be precise, $\{\epsilon_t\}_{t\in\mathbb{N}}$ is a Gaussian discrete white noise, and in case the stock price follows the fundamental price, ϵ_{t+1} represents the logarithmic return from period t to $t+1$.

As in Day and Huang [13] and Tramontana et al. [47], we assume that a market maker adjusts prices in the direction of excess demand by mediating out-of-equilibrium transactions. Namely, the log of price P for period $t+1$ which is quoted by the market maker is given by:

$$P_{t+1} = P_t + a\left(D_t^{C,1} + D_t^{C,2} + D_t^{F,1} + D_t^{F,2} + D_t^{T}\right) + \epsilon_{t+1} \tag{2}$$

where a is a positive price adjustment parameter (measuring market power of traders) and, being a scaling parameter, in the following is set equal to one without loss of generality. Moreover, at a generic time t, $D_t^{C,1}$ and $D_t^{C,2}$ denote the demands of asset by type 1 chartists and by type 2 chartists, respectively, while $D_t^{F,1}$ and $D_t^{F,2}$ are the orders placed by type 1 fundamentalists and by type 2 fundamentalists, respectively, and finally, the order placed by the trend following trader is indicated by D_t^T. In addition, the market price is affected by the fundamental shocks. Hence, excluding fundamental shocks, prices increase when traders' buying orders exceed traders' selling orders, and vice versa. This is a well-known price adjustment mechanism which is commonly used in behavioral finance, see, e.g., Beja and Goldman [6], Day and Huang [13] and Farmer and Joshi [20].

As in Day and Huang [13] and Tramontana et al. [47], chartists expect bull and bear markets to continue. Specifically, the demand of assets by the first type of chartists is given by

$$D_t^{C,1} = \begin{cases} c^{1,a}\,(P_t - F_t) & \text{if } P_t - F_t \geq 0 \\ c^{1,b}\,(P_t - F_t) & \text{if } P_t - F_t < 0 \end{cases} \tag{3}$$

where $c^{1,a}$ and $c^{1,b}$ are positive reaction parameters. Therefore, type 1 chartists submit buying orders in a bull market (the asset price is above the fundamental value) and selling orders in a bear market (the asset price is below the fundamental value). The size of these orders may depend on market conditions. For instance, for $c^{1,a} > c^{1,b}$ this type of traders trades more heavily in a bull market than in a bear market. Empirical findings supporting the existence of such an asymmetric propensity to trade can be found, for example, in Boswijk et al. [8].

Similarly, the demand of assets by type 2 chartists is given by

$$D_t^{C,2} = \begin{cases} c^{2,a} & \text{if } P_t - F_t > 0 \\ 0 & \text{if } P_t - F_t = 0 \\ -c^{2,b} & \text{if } P_t - F_t < 0 \end{cases} \tag{4}$$

which means that the buying order is given by $c^{2,a} > 0$ in a bull market, while in a bear market chartists of type 2 sell instead of buying, and the selling order is given by $c^{2,b} > 0$. Thus, unlike the trading rules of chartists of type 1, the magnitude of the deviation of the market price from the fundamental value of the asset does not impact on the size of the orders placed by chartists of type 2. This is the only difference between chartists of type 1 and chartists of type 2. In the (special) case of prices equal to the fundamental value, type 2 chartists do not submit orders.

An opposite trading strategy is adopted by fundamentalists, who believe that prices return to their fundamental value in the long run. Specifically, the demand of

assets placed by type 1 fundamentalists (mean reverter fundamentalists) is given by

$$D_t^{F,1} = \begin{cases} f^{1,a}\,(F_t - P_t) & \text{if } F_t - P_t \geq 0 \\ f^{1,b}\,(F_t - P_t) & \text{if } F_t - P_t < 0 \end{cases} \tag{5}$$

where $f^{1,a}$ and $f^{1,b}$ are positive reaction parameters. Therefore, fundamentalists of type 1 sell (buy) assets when the prices are above (below) the fundamental value because the market is regarded as overvalued (undervalued), see, e.g., Brock and Hommes [10] or Lux [31]. The demand of assets of fundamentalists of type 1 is proportional to the difference between market price and fundamental price, and this type of trader reacts asymmetrically to bear and bull markets when $f^{1,a}$ and $f^{1,b}$ are unequal.

Similarly, the demand of assets placed by type 2 fundamentalists is given by

$$D_t^{F,2} = \begin{cases} f^{2,a} & \text{if } F_t - P_t > 0 \\ 0 & \text{if } F_t - P_t = 0 \\ -f^{2,b} & \text{if } F_t - P_t < 0 \end{cases} \tag{6}$$

Therefore, when the market is undervalued, fundamentalists of type 2 buy $f^{2,a}$ (> 0) assets. They sell $f^{2,b}$ (> 0) assets when the market is overvalued and they do not trade in the particular case in which the market price mirrors its fundamental value.

Finally, the orders placed by trend followers are defined as

$$D_t^{T} = \begin{cases} d_{\mathrm{R}}\,(P_t - P_{t-1}) & \text{if } P_t - F_t > 0 \\ 0 & \text{if } P_t - F_t = 0 \\ d_{\mathrm{L}}\,(P_t - P_{t-1}) & \text{if } P_t - F_t < 0 \end{cases} \tag{7}$$

where $d_{\mathrm{R}}, d_{\mathrm{L}} > 0$. Hence, the trend follower submits buying (selling) orders in an upward (downward) price trend. Note that the size of these orders may be asymmetric with respect to a bull or bear market situation, therefore capturing a sentimental component. For instance, for $d_{\mathrm{R}} > d_{\mathrm{L}}$ this type of traders bets more heavily in a bull market than in a bear market. In the particular case in which the most recent price is equal to the fundamental value, this type of traders does not trade.[1]

The trading strategies in (3)–(7) represent simple behavioral rules, and we show that such simple trading strategies are sufficient to alter the distribution of the returns generated by the fundamental process (represented by a classical random walk) and generate interesting price dynamics that shows some of the stylized facts observed in the financial market. Specifically, substituting trading strategies (3)–(7) in (2), we have that the log price of the stock market follows the (random) dynamical system:

$$\begin{aligned} P_{t+1} &= P_t + \epsilon_{t+1} \\ &+ \begin{cases} c^{1,a}\,(P_t - F_t) + f^{1,b}\,(F_t - P_t) + c^{2,a} - f^{2,b} + d_{\mathrm{R}} P_t - d_{\mathrm{R}} P_{t-1} & \text{if } P_t - F_t > 0 \\ 0 & \text{if } P_t - F_t = 0 \\ c^{1,b}\,(P_t - F_t) + f^{1,a}\,(F_t - P_t) - c^{2,b} + f^{2,a} + d_{\mathrm{L}} P_t - d_{\mathrm{L}} P_{t-1} & \text{if } P_t - F_t < 0 \end{cases} \end{aligned} \tag{8}$$

and the logarithmic returns of the stock market are therefore given by

$$P_{t+1} - P_t = \epsilon_{t+1} + \begin{cases} \left(c^{1,a} - f^{1,b} + d_{\mathrm{R}}\right) P_t + \left(f^{1,b} - c^{1,a}\right) F_t - d_{\mathrm{R}} P_{t-1} + c^{2,a} - f^{2,b} & \text{if } P_t - F_t > 0 \\ 0 & \text{if } P_t - F_t = 0 \\ \left(c^{1,b} - f^{1,a} + d_{\mathrm{L}}\right) P_t + \left(f^{1,a} - c^{1,b}\right) F_t + f^{2,a} - c^{2,b} - d_{\mathrm{L}} P_{t-1} & \text{if } P_t - F_t < 0 \end{cases} \tag{9}$$

For simplicity of notation, let us define the aggregate parameters as

$$s_{\mathrm{R}} = c^{1,a} - f^{1,b}, \quad s_{\mathrm{L}} = c^{1,b} - f^{1,a} \tag{10}$$

and the constant terms as

$$m_{\mathrm{R}} = c^{2,a} - f^{2,b}, \quad m_{\mathrm{L}} = f^{2,a} - c^{2,b} \tag{11}$$

Then, we obtain

$$P_{t+1} - P_t = \epsilon_{t+1}$$

[1] An alternative modeling choice is represented by assuming that this type of trader adopts with probability one-half the trading strategy employed in the bull market and with probability one-half the trading strategy employed in the bear market every time the market price coincides with the fundamental price, i.e., he adopts the trend following strategy using an extrapolation rate which is the average of the extrapolation rates used in the bear and the bull markets. This alternative modeling choice would impact the dynamics of the deterministic skeleton of the model only in a zero-measure subset of the state space as discussed in the next section.

$$+\begin{cases}(d_{\mathrm{R}}+s_{\mathrm{R}})\,P_t-s_{\mathrm{R}}F_t-d_{\mathrm{R}}P_{t-1}+m_{\mathrm{R}} & \text{if } P_t-F_t>0\\ 0 & \text{if } P_t-F_t=0\\ (d_{\mathrm{L}}+s_{\mathrm{L}})\,P_t-s_{\mathrm{L}}F_t-d_{\mathrm{L}}P_{t-1}+m_{\mathrm{L}} & \text{if } P_t-F_t<0\end{cases} \tag{12}$$

The aggregate parameter s_{R} measures how chartists of type 1 trade more aggressively than mean reverter fundamentalists (or fundamentalists of type 1) in the bull market. Specifically, $s_{\mathrm{R}}>0$ means that in a bull market chartists of type 1 are more aggressive than fundamentalists of type 1 and the mean-fleeing component prevails, $s_{\mathrm{R}}=0$ means that in a bull market the trading strategy of chartists of type 1 offsets one of the fundamentalists of type 1, finally, $s_{\mathrm{R}}<0$ means that in a bull market chartists of type 1 are less aggressive than fundamentalists of type 1, and the mean-reverting component prevails. A similar but opposite effect is played by the parameter s_{L} but in a bear market. The parameter m_{R} measures how chartists of type 2 trade more aggressively than fundamentalists of type 2. Specifically, in a bull market the buying orders of chartists of type 2 prevail the selling orders of fundamentalists of type 2 when $m_{\mathrm{R}}>0$, the trading strategy of chartists of type 2 is counterbalanced by the trading strategy of fundamentalists of type 2 so that the combined strategies do not produce any price effect when $m_{\mathrm{R}}=0$, and finally, the buying orders of chartists of type 2 are more than compensated by the selling orders of fundamentalists of type 2 when $m_{\mathrm{R}}<0$. A similar but opposite effect is played by the parameter m_{L} but in a bear market. The parameters d_{R} and d_{L} measure how active are the trend following traders in a bull market and in a bear market, respectively.

Denoting the logarithmic return of the asset at time $t+1$ by $r_{t+1}=P_{t+1}-P_t$, we observe that the asset pricing model in (12) implies that in a bull market the returns of the asset follow an autoregressive process of order one (AR(1) process) plus a behavioral component

$$r_{t+1}=\underbrace{d_{\mathrm{R}}r_t+\epsilon_{t+1}+m_{\mathrm{R}}}_{AR(1)}+\underbrace{s_{\mathrm{R}}\,(P_t-F_t)}_{B(P_t)} \tag{13}$$

where the behavioral component in the dynamics of the asset returns is given by $B\,(P_t)$. The same type of process (with different parameters) takes place in a bear market. Since an autoregressive process is not able to replicate the empirical stylized facts that our model is able to replicate, we can attribute these features to the behavioral components and to the asymmetric trading attitudes between bear and bull markets.

3 The deterministic skeleton of the model

Setting $\sigma_F=0$, we obtain the deterministic skeleton of the asset pricing model (8), which is a simple two-dimensional discontinuous map. Moreover, operating the change of variable $x_t=P_t-F$, we obtain

$$x_{t+1}=\begin{cases}(1+d_{\mathrm{R}}+s_{\mathrm{R}})\,x_t-d_{\mathrm{R}}x_{t-1}+m_{\mathrm{R}} & \text{if } x_t>0\\ (1+d_{\mathrm{L}}+s_{\mathrm{L}})\,x_t-d_{\mathrm{L}}x_{t-1}+m_{\mathrm{L}} & \text{if } x_t<0\end{cases} \tag{14}$$

knowing that for $x_t=0$, we assume the fundamental value and thus $x_{t+1}=0$. In addition, by introducing the lagged variable $y_t=x_{t-1}$, the system can be represented by the following map T

$$T:\begin{pmatrix}x_{t+1}\\ y_{t+1}\end{pmatrix}=\begin{cases}T_{\mathrm{R}}(x_t,y_t)=\begin{pmatrix}t_{\mathrm{R}} & -d_{\mathrm{R}}\\ 1 & 0\end{pmatrix}\begin{pmatrix}x_t\\ y_t\end{pmatrix}+\begin{pmatrix}m_{\mathrm{R}}\\ 0\end{pmatrix} & \text{if } x_t>0\\ T_{\mathrm{L}}(x_t,y_t)=\begin{pmatrix}t_{\mathrm{L}} & -d_{\mathrm{L}}\\ 1 & 0\end{pmatrix}\begin{pmatrix}x_t\\ y_t\end{pmatrix}+\begin{pmatrix}m_{\mathrm{L}}\\ 0\end{pmatrix} & \text{if } x_t<0\end{cases} \tag{15}$$

where

$$t_{\mathrm{R}}=1+d_{\mathrm{R}}+s_{\mathrm{R}},\quad t_{\mathrm{L}}=1+d_{\mathrm{L}}+s_{\mathrm{L}} \tag{16}$$

Notice that by a linear scaling of the state variable and parameters, we can get rid of one parameter, allowing for example to settle $m_{\mathrm{R}}=1$ or $m_{\mathrm{L}}=1$, but we prefer to keep the map in its complete definition of parameters for reasons that will be clarified in the following: the symmetry (here intended as interchangeability of the L/R symbols) of the two linear functions $T_{\mathrm{L}}\,(x_t,y_t)$ and $T_{\mathrm{R}}\,(x_t,y_t)$ will be used in determining the equations of the bifurcation sets.

By using the unit time advancement operator "$'$" we can also write $(x',y')=T\,(x,y)$ and we can consider, without loss of generality, map T as defined in the two partitions, L and R, representing the half planes $x<0$ and $x>0$, respectively, without specifying any value for the case $x=0$. Thus, the asset pricing model can be written as a *two-dimensional piecewise linear* and, in general, discontinuous map $T\,(x,y)$, where the parameters $t_{\mathrm{R}},m_{\mathrm{R}},t_{\mathrm{L}},m_{\mathrm{L}}\in\mathbb{R}$ (as defined in (10), (11), (16)) and we assume $d_{\mathrm{R}},d_{\mathrm{L}}\geq 0$.

For an invariant set, in particular for a periodic point of a k-cycle, the collision with $x=0$ always corresponds to a border collision, such a point is mapped by both functions $T_{\mathrm{L}}\,(x,y)$ and $T_{\mathrm{R}}\,(x,y)$ into a point of the line $y=0$, and this occurrence must be dealt separately.

The switching manifold of map $T\,(x,\,y)$ is the line $x = 0$, on which we do not consider any definition, as in fact it does not alter the analysis that we perform in this work, where this line, being the border at which map T changes definition, is the one involved in border collision bifurcations of invariant sets of map T. In the formulation of the model, as commented above, we are interested in the trajectory of any point of the x-axis, including in particular, the origin $O = (0, 0)$ which represents the fundamental stationary state, and it is a fixed point never reached when the map is discontinuous with $m_{\rm L} \neq 0$ and $m_{\rm R} \neq 0$.

As already remarked, a first consideration is that the map T is in general discontinuous. In fact, considering a generic linear map with trace t and determinant d in the form

$$M\,(x,\,y) = \begin{pmatrix} t & -d \\ 1 & 0 \end{pmatrix} \begin{pmatrix} x \\ y \end{pmatrix} + \begin{pmatrix} m \\ 0 \end{pmatrix} \tag{17}$$

we have that the set $x = 0$ is mapped into the line $y = 0$, that is, a point $(0,\,y)$ is mapped into $(-dy + m, 0)$ so that, if we do not consider the origin, map T is continuous iff $d_{\rm L} = d_{\rm R}$ and $m_{\rm L} = m_{\rm R}$, in which case it is topologically conjugate to the standard two-dimensional normal form (see, e.g., [40] and [45]) and the origin is a fixed point only for $m = 0$.

That is, for $d_{\rm L} = d_{\rm R} = d$ and $m_{\rm L} = m_{\rm R} = 0$ the map T is continuous and the fundamental stationary state, $O = (0, 0)$, is a fixed point. This particular case has already been investigated in the literature. It has been observed that also fixing the determinant $d < 1$ and the two traces $t_{\rm R}$ and $t_{\rm L}$ such that the origin is attracting for both linear maps $T_{\rm R}$ and $T_{\rm L}$, the map T may have almost all the trajectories divergent, as remarked in several papers ([3,17,42]), where the so-called *dangerous bifurcations* have been studied, or (depending on the values of the parameters) the origin is globally attracting.

Differently, the particular cases: $d_{\rm L} = d_{\rm R} = d$, $m_{\rm L} = m_{\rm R} = 0$ and $t_{\rm R} = t_{\rm L} = t$ lead to a continuous linear map with fixed point $O = (0, 0)$, so that its dynamics are well known. Let us consider values of t (the trace) and d (the determinant) such that the fixed point is attracting. Due to the linearity, it is globally attracting, but, as we shall see, the dynamics change drastically when we move to a discontinuous map (even if the two definitions $T_{\rm L}$ and $T_{\rm R}$ are separately affine maps with attracting fixed points).

So, let us consider the fixed point of the generic map M, which is given by $P^* = (x^*,\,y^*)$ with

$$x^* = y^* = \frac{m}{1 - t + d} \tag{18}$$

The eigenvalues $\lambda_{1,2}$ of the Jacobian matrix are $\lambda_{1,2} = \frac{1}{2}\left(t \pm \sqrt{t^2 - 4d}\right)$, and when they are real a couple $r_{1,2}$ of related eigenvectors is given by

$$r_{1,2} = \begin{pmatrix} 1 \\ 1/\lambda_{1,2} \end{pmatrix} \tag{19}$$

The stability of the fixed point $P^* = (x^*,\,y^*)$ of map M depends on the values of the parameters trace t and determinant d. Necessary and sufficient conditions for the asymptotic stability are $d < 1$, $1 - t + d > 0$ and $1 + t + d > 0$, which identify the well-known stability triangle in the parameter plane (t, d), the boundaries of which are given by the curves of equations $d = 1$, $1 - t + d = 0$ and $1 + t + d = 0$. Moreover, the Jacobian has complex eigenvalues for $t^2 - 4d < 0$.

In terms of the parameters (s, d) of our system, where $t = 1 + d + s$, we obtain

$$x^* = y^* = \frac{m}{-s} \tag{20}$$

Therefore, map T has a real fixed point (*bear market equilibrium*) $P^*_{\rm L} = \left(x^*_{\rm L}, x^*_{\rm L}\right)$ iff $x^*_{\rm L} = \frac{m_{\rm L}}{1 - t_{\rm L} + d_{\rm L}} = \frac{m_{\rm L}}{-s_{\rm L}} < 0$, otherwise we say that $P^*_{\rm L}$ is a virtual fixed point. Similarly, map T has a real fixed point (*bull market equilibrium*) $P^*_{\rm R} = \left(x^*_{\rm R}, x^*_{\rm R}\right)$ iff $x^*_{\rm R} = \frac{m_{\rm R}}{1 - t_{\rm R} + d_{\rm R}} = \frac{m_{\rm R}}{-s_{\rm R}} > 0$; otherwise, we say that $P^*_{\rm R}$ is virtual. A fixed point undergoes a border collision when either $x^*_{\rm R} = 0$ or $x^*_{\rm L} = 0$.

The stability of a fixed point $P^* = (x^*,\,y^*)$ in terms of the parameters (s, d) of our system, where $s = -1 + t - d$, can be rewritten as follows $d < 1$, $s < 0$, $d > -1 - \frac{s}{2}$, and the stability triangle in the parameter plane (s, d) is shown in Fig. 1, bounded by the curves of equation $d = 1$, $s = 0$, $d = -1 - \frac{s}{2}$, and the region with complex eigenvalues becomes $s^2 + 2s(1 + d) + (1 - d)^2 < 0$, bounded by the curves $s = -(1 - d) \pm 2\sqrt{d}$ for $d > 0$.

The inverse of the linear map $M\,(x,\,y)$ is given by

$$M^{-1}\,(u,\,v) = \left(v,\,\frac{-u + tv + m}{d}\right) \tag{21}$$

so that, in particular, we have that $M^{-1}(0, v)$ is the line of equation $y = \frac{tx + m}{d}$, and the preimage of the switching line $x = 0$ for map T consists in two half-lines:

$$\begin{cases} y = \frac{t_{\rm R} x + m_{\rm R}}{d_{\rm R}} & \text{if } x > 0 \\ y = \frac{t_{\rm L} x + m_{\rm L}}{d_{\rm L}} & \text{if } x < 0 \end{cases} \tag{22}$$

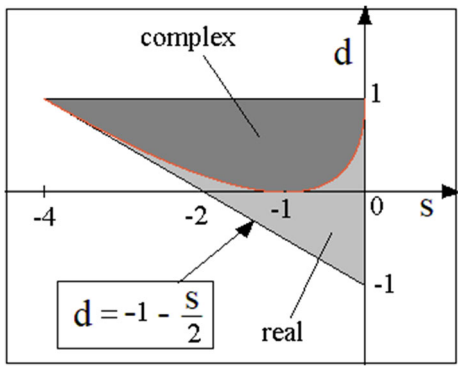

Fig. 1 Stability region in the (s, d) parameter plane for the equilibrium $(x^*, y^*) = \left(\frac{m}{-s}, \frac{m}{-s}\right)$ of the map M in (17)

Moreover, since we assume that map T has both determinants with positive signs, the resulting map is invertible for $y \neq 0$ and, as it is immediate to see, the left (respectively, right) side is mapped by T into the half plane below (respectively, above) $y = 0$,

$$T^{-1}(u, v) = \begin{cases} T_{\mathrm{R}}^{-1}(u, v) = (v, \frac{-u+t_{\mathrm{R}}v+m_{\mathrm{R}}}{d_{\mathrm{R}}}) & \text{if } v > 0 \\ T_{\mathrm{L}}^{-1}(u, v) = (v, \frac{-u+t_{\mathrm{L}}v+m_{\mathrm{L}}}{d_{\mathrm{L}}}) & \text{if } v < 0 \end{cases} \tag{23}$$

as qualitatively shown in Fig. 2.

Clearly a point of $y = 0$ say $(z, 0)$ can be obtained by applying either the function T_{L} or T_{R} so that we can say that such a point may have an inverse with T_{L}^{-1} or with T_{R}^{-1}, but notice that such cases are considered always as bifurcation situations, which are handled separately. That is, when an invariant set, typically a cycle, has a point which is colliding with $x = 0$, then the set also collides with $y = 0$, and it is known if the cycle is obtained by applying T_{L} or T_{R}.

As we have already remarked, when the parameters are set such that both linear functions T_{L} and T_{R} have a real attracting fixed point in the origin and map T is continuous, then there are wide regions in the parameter space (s, d) leading to a fundamental value which is globally attracting. However, when map T is discontinuous, several different dynamic behaviors may be observed and explained. Let us consider first an example in which we fix the values of the parameters of the map so as to have two attracting fixed points with complex eigenvalues, for example

$$\begin{aligned} &d_{\mathrm{L}} = 0.5,\ s_{\mathrm{L}} = -0.4 \text{ (so that } t_{\mathrm{L}} = 1.1) \text{ and } d_{\mathrm{R}} = 0.4, \\ &s_{\mathrm{R}} = -0.5 \text{ (so that } t_{\mathrm{L}} = 0.9), \end{aligned} \tag{24}$$

and let us consider the two-dimensional parameter plane $(m_{\mathrm{R}}, m_{\mathrm{L}})$. Clearly for $m_{\mathrm{R}} > 0$ and $m_{\mathrm{L}} < 0$ both fixed points exist, as attracting foci, and the phase plane has at least two coexisting attracting sets; an example is shown in Fig. 3a at $m_{\mathrm{R}} = 0.1$ and $m_{\mathrm{L}} = -0.1$, which also shows the two basins of attraction, which are separated by the preimages of segments of the critical line LC (or discontinuity line) $x = 0$ (the first segments of LC_{-1} are also evidenced in gray in the figure).

Also we know that if we change the value m_{R} from positive to negative, then the fixed point P_{R}^* crosses $x = 0$ becoming virtual; similarly if we change the value m_{L} from negative to positive, then the fixed point P_{L}^* crosses $x = 0$ becoming virtual. It is interesting to see that when only one fixed point becomes virtual, the other existing one may coexist with an attracting cycle. For example, at $m_{\mathrm{R}} = 0.05$ and $m_{\mathrm{L}} = 2$, P_{L}^* is virtual, and the attracting fixed point P_{R}^* coexists with an attracting 5-cycle, having symbolic sequence LR^4, or at $m_{\mathrm{R}} = -1$ and $m_{\mathrm{L}} = -0.05$, P_{R}^* is virtual, and the attracting fixed point P_{L}^* coexists with an attracting 6-cycle, having symbolic sequence RL^5, whose basins are separated by the preimages of segments of the discontinuity line $x = 0$, as shown in Fig. 3b. Indeed, since changes in m_{R} and m_{L} do not involve trace and determinant of the two linear matrices, the determinants are always smaller than 1 in all the points of the plane, for any composition of the two functions T_{L} and T_{R} so that expanding cycles cannot exist, and if the eigenvalues persist as complex ones, then it is plausible that the system cannot have saddle cycles, that is, only attracting cycles are allowed, which may coexist, and the related basins of attraction are bounded only by preimages of segments belonging to the discontinuity line $x = 0$. Notice that the number of coexisting attracting cycles in PWL maps can also be infinite, see Simpson [41] and Simpson and Tuffley [44].

The coexistence of a stable fixed point and an attracting cycle cannot be observed for $d_{\mathrm{R}} = d_{\mathrm{L}} = 0$, i.e., when the trend follower traders are out of the market and the map T reduces to a one-dimensional map, see Tramontana et al. [47]. This peculiarity of our two-dimensional model is relevant as the literature on heterogeneous asset pricing models shows that forcing by a random noise a nonlinear model characterized by the coexistence of a stable fixed point and a cyclical attractor, it is possible to replicate an important stylized fact such as the volatility clustering effect.

Given its theoretical and application relevance, let us further underline this point. In the one-dimensional case, when the eigenvalues (slopes of the two linear

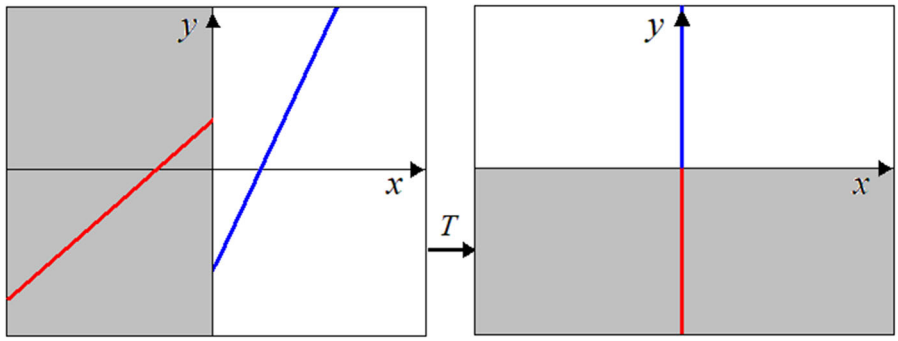

Fig. 2 Qualitative representation of the action of map T. The red line is the preimage of the set $x = 0$ from the left; the blue region is the preimage of the set $x = 0$ from the right; in the case d_R, d_L, t_R, t_L positive, $m_R < 0$ and $m_L > 0$. The gray areas show how the map transforms the left half plane in one iteration, and the white regions show how the map transforms the right half plane in one iteration

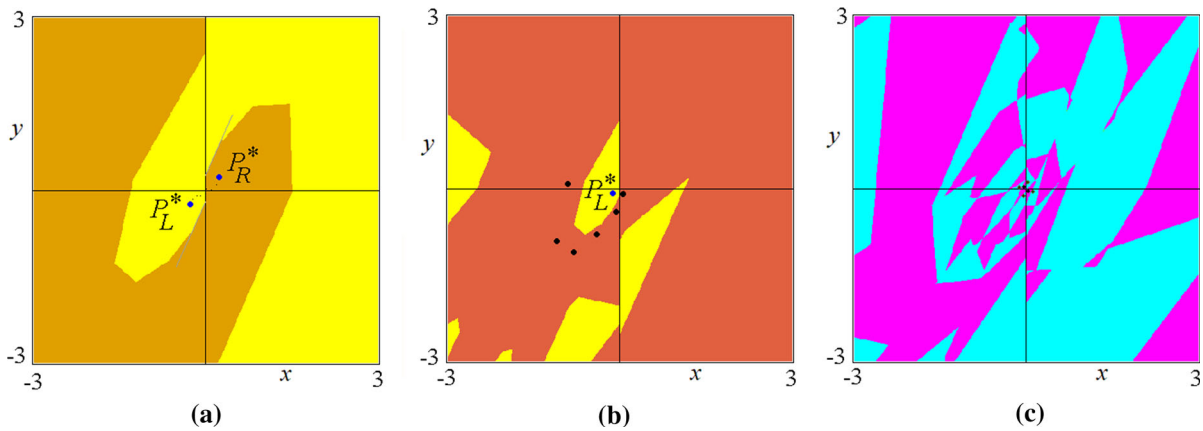

Fig. 3 Graphic representation of the subregion $(-3, 3) \times (-3, 3)$ of the phase space of the map T. The yellow region represents the basin of attraction of the bear market equilibrium $\left(x_L^*, y_L^*\right)$, the orange region represents the basin of attraction of the bull market equilibrium $\left(x_R^*, y_R^*\right)$, the red region represents the basin of attraction of the 6-period cycle with symbolic sequence RL^5, the magenta region represents the basin of attraction of the 2-period cycle with symbolic sequence RL and the azure region represents the basin of attraction of a 4-period cycle with symbolic sequence R^2L^2. The parameters d_L, s_L, d_R and s_R are as in (24). Panel (**a**) $m_L = -0.1$ and $m_R = 0.1$. Panel (**b**) $m_L = -0.05$ and $m_R = -1$. Panel (c), $m_L = 0.1$ and $m_R = -0.1$

functions) are positive and smaller than 1, then the parameter range in which the two fixed points are both virtual is filled with periodicity regions organized in the period adding bifurcation structure. That is, only attracting cycles can exist and the periods and rotation numbers of the existing attracting cycles in the bifurcation structure follow the *Farey summation rule*. Moreover, the symbolic sequences of the cycles in the bifurcation structure are obtained by concatenation of sequences, starting from those of the so-called basic cycles, given by LR^n and RL^n for $n \geq 1$, and their peculiarity is that the periodicity regions cannot overlap, so that coexistence of cycles is not possible in the one-dimensional case. It was conjectured that similar bifurcation structures also exist in two-dimensional discontinuous PWL maps (see, e.g., [34] and [43]). Thus, we also were looking for a similar bifurcation structure. However, in our system (map T), although periodicity regions Π_{LR^n} and Π_{RL^n} associated with the existence of attracting basic cycles, LR^n and RL^n for some n, can be found, what is observed as a generic behavior is the overlapping of periodicity regions, lead-

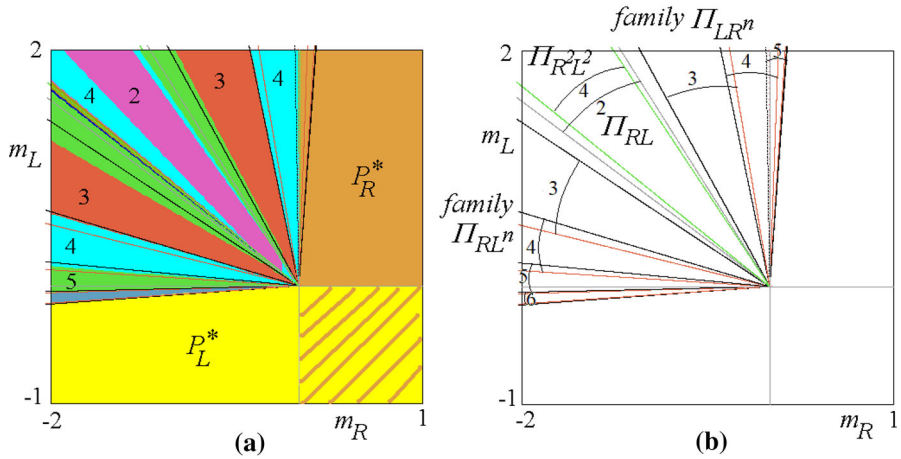

Fig. 4 Two-dimensional bifurcation diagram of the map T with respect to the parameter plane $(m_\mathrm{R}, m_\mathrm{L})$. The shaded area $\{(m_\mathrm{R}, m_\mathrm{L}) : d_\mathrm{L}, d_\mathrm{R} < 0\}$ indicates that the bull market equilibrium and the bear market equilibrium coexist stable. The yellow region indicates that the bear market equilibrium is the unique attractor, while the bull market equilibrium is virtual. The orange region indicates that the bull market equilibrium is the unique attractor, while the bear market equilibrium is virtual. The straight lines coming out of the origin are the border collision bifurcation curves and mark the regions of existence of the basic cycles with symbolic sequences RL^n and LR^n, with $n = 2, \ldots, 6$ as indicated in Panel (b). The two-dimensional bifurcation diagram has been obtained with the parameters as in (24), in red for parameters as in (39) and in black for parameters as in (41)

ing to coexistence of several different attracting cycles. Moreover, while in the one-dimensional case the periodicity regions Π_{LR^n} and Π_{RL^n} are separated in the parameter space (so that in the first family of cycles (LR^n with $n \geq 1$), two consecutive symbols L are not allowed, and similarly in the second family of cycles (RL^n with $n \geq 1$) two consecutive symbols R cannot exist), in the two-dimensional case this is no longer forbidden. In particular, when an attracting 2-cycle exists, with symbolic sequence LR, then we may found also a coexisting attracting 4-cycle with symbolic sequence L^2R^2. An example is shown in Fig. 3c at $m_\mathrm{R} = -0.1$ and $m_\mathrm{L} = 0.1$: the two fixed points are both virtual and an attracting 2-cycle coexists with an attracting 4-cycle L^2R^2, whose basins are also shown in the figure.

A two-dimensional bifurcation diagram in the $(m_\mathrm{R}, m_\mathrm{L})$ parameter plane, as shown in Fig. 4a, can immediately show the existence and coexistence of periodicity regions of attracting cycles, and we give in the next section the equations of the BCB conditions leading to the boundaries of the regions for the basic cycles. Let us remark that detecting these regions of the basic cycles is particularly relevant from the application point of view. In fact, they allow to identify the regions of the parameter space characterized by coexisting attractors and this helps to study the conditions under which the stochastic version of the model is able to replicate the empirical stylized facts characterizing the financial markets. In the following, we identify only the BCB curves, while the existence of these bifurcations is verified numerically. Therefore, the conditions that follow have to be interpreted as necessary conditions for the existence of the BCBs and of the cycles that these bifurcations originate.

3.1 BCB conditions

3.1.1 2-cycle

Let us first consider the conditions for the 2-cycle with symbolic sequence LR and for the 4-cycle with symbolic sequence L^2R^2. For the 2-cycle, we have to determine a fixed point of the second iterate of the map, say $T_\mathrm{L} \circ T_\mathrm{R}\,(x, y) = (x, y)$ leading to a point $(x_\mathrm{R}, y_\mathrm{R})$ with $x_\mathrm{R} > 0$ and as well $T_\mathrm{R} \circ T_\mathrm{L}\,(x, y) = (x, y)$ leading to a point $(x_\mathrm{L}, y_\mathrm{L})$ with $x_\mathrm{L} < 0$. The existence region of such a 2-cycle is bounded by BCB curves, the first one is obtained by the collision with the line $x = 0$ from the periodic point on the right side, while the second one is obtained by the collision with the line $x = 0$ from the periodic point on the left side. There-

fore, when $T_L \circ T_R(0, y_R) = (0, y_R)$ is satisfied, the first BCB occurs; when $T_R \circ T_L(0, y_L) = (0, y_L)$ is satisfied, the second BCB occurs. Considering

$$T_L \circ T_R \begin{pmatrix} x \\ y \end{pmatrix} = \begin{pmatrix} x(t_L t_R - d_L) - t_L d_R y + t_L m_R + m_L \\ t_R x - d_R y + m_R \end{pmatrix} \quad (25)$$

the condition $T_L \circ T_R(x, y) = (x, y)$ leads to

$$x_R = x_R^{RL} = \frac{t_L m_R + (1 + d_R) m_L}{(1 + d_R)(1 + d_L) - t_L t_R},$$
$$y_R = y_R^{RL} = \frac{t_R x_R + m_R}{1 + d_R} \quad (26)$$

which requires that the numerator and denominator of x_R^{RL} have the same sign and the denominator needs to be different from zero to have x_R^{RL} that exists and it is larger than zero. Then, $x_R^{RL} = 0$ occurs for

$$m_L = -\frac{t_L}{1 + d_R} m_R \quad (27)$$

To obtain the other periodic point of the possible 2-cycle, we can clearly compute $(x_L, y_L) = T_R(x_R, y_R)$. However, due to the symmetry between the two functions T_L and T_R with respect to the symbols L/R, we have that to get the conditions for $T_R \circ T_L(x, y) = (x, y)$ it is enough to exchange L/R in the expressions given above, so that for the other border collision condition we get:

$$x_L = x_L^{LR} = \frac{t_R m_L + (1 + d_L) m_R}{(1 + d_R)(1 + d_L) - t_L t_R},$$
$$y_L = y_L^{LR} = \frac{t_L x_L + m_L}{1 + d_L} \quad (28)$$

which requires that the numerator and denominator of x_L^{LR} have opposite sign and the denominator needs to be different from zero to have x_L^{LR} that exists and it is smaller than zero. Then, $x_L^{LR} = 0$ occurs for $m_R = -\frac{t_R}{1+d_L} m_L$, that is

$$m_L = -\frac{1 + d_L}{t_R} m_R \quad (29)$$

These two conditions in the (m_R, m_L) parameter plane lead to two straight lines issuing from the origin and with negative slopes (since we have both traces and determinants with positive signs), leading to the existing region of the 2-cycle when both fixed points are virtual. These BCB curves are plotted in Fig. 4b.

3.1.2 4-cycle L^2R^2

We can reason similarly to obtain the existence conditions for the 4-cycle L^2R^2. Here we have to consider first the functions of the second iterate: $T_R^2(x, y) = T_R \circ T_R(x, y)$ and $T_L^2(x, y) = T_L \circ T_L(x, y)$. Straightforward computations lead to

$$T_R^2 \begin{pmatrix} x \\ y \end{pmatrix} = \begin{pmatrix} x(t_R^2 - d_R) - t_R d_R y + t_R m_R + m_R \\ t_R x - d_R y + m_R \end{pmatrix} \quad (30)$$

and for $T_L^2(x, y)$ it is enough to change the symbol R into L. Then, the composition $T_L^2 \circ T_R^2(x, y) = (x, y)$ leads to a point (x_R^1, y_R^1) which may belong to a 4-cycle, which undergoes a BCB when $x_R^1 = 0$ occurs. This gives the condition

$$m_L = -m_R \frac{d_L^2(t_R + d_R) + t_L(1 + t_R) + d_L}{t_L^2(t_L + d_L) + 1 - d_L d_R - t_L d_R - t_R d_L} \quad (31)$$

and similarly from $T_R^2 \circ T_L^2(x, y) = (x, y)$ a periodic point on the L side is obtained which may belong to a 4-cycle undergoing a BCB when it holds

$$m_L = -m_R \frac{t_R^2(t_R + d_R) + 1 - d_L d_R - t_R d_L - t_L d_R}{d_R^2(t_L + d_L) + t_R(1 + t_L) + d_R} \quad (32)$$

These curves are plotted in Fig. 4b.

3.1.3 Basic cycles

From Fig. 4, we can see that when the fixed point P_L^* is virtual and P_R^* is an attracting focus, decreasing m_R toward 0 an attracting 5-cycle appears, coexisting with P_R^*, see Fig. 5a at $m_R = 0.12$ and $m_L = 2$. The colliding periodic point as a fixed point of $T_R^4 \circ T_L(x, y)$ collides with $x = 0$, or, equivalently as a fixed point of $T_L \circ T_R^4(x, y)$ collides with $y = 0$. Thus, to get the BCB we can solve for $T_R^4 \circ T_L(x, y) = (x, y)$ and then consider $x = 0$, or we can solve for $T_L \circ T_R^4(x, y) = (x, y)$ and then consider $y = 0$.

Decreasing m_R also the fixed point P_R^* becomes virtual and the attraction 5-cycle with symbolic sequence LR^4 is attracting, undergoing a border collision when the periodic point on the right side closest to $x = 0$ collides with $x = 0$ and the unique point of the left side collides with $y = 0$. In Fig. 5b at $m_R = -0.02$ and $m_L = 2$, the 5-cycle is close to the bifurcation leading to its disappearance, and an attracting 4-cycle with

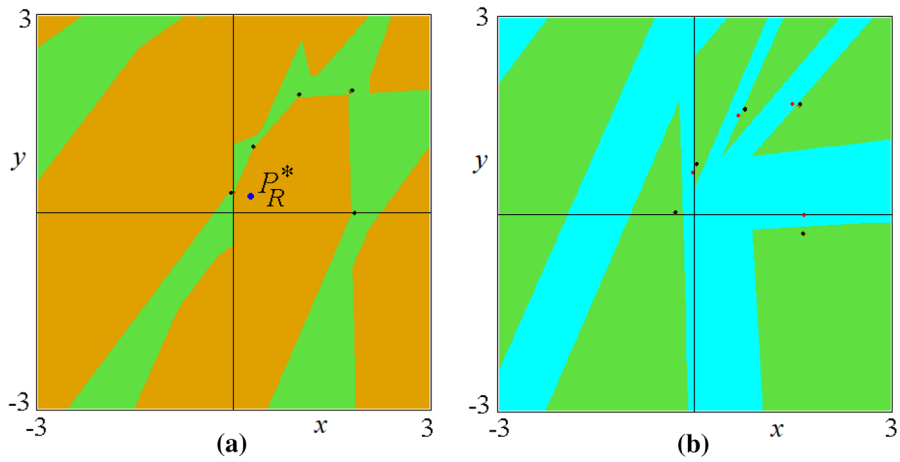

Fig. 5 Graphic representation of the subregion $(-3, 3)\times(-3, 3)$ of the phase space of the map T. The orange region represents the basin of attraction of the bull market equilibrium $\left(x_{\mathrm{R}}^*, y_{\mathrm{R}}^*\right)$, the green region represents the basin of attraction of the 5-period cycle with symbolic sequence LR^4, and the azure region represents the basin of attraction of a 4-period cycle with symbolic sequence LR^3. The parameters d_{L}, s_{L}, d_{R} and s_{R} are as in (24). Panel (a), $m_{\mathrm{L}} = 2$ and $m_{\mathrm{R}} = 0.12$. Panel (b), $m_{\mathrm{L}} = 2$ and $m_{\mathrm{R}} = -0.02$. Compare with Fig. 3

symbolic sequence LR^3 just appeared. So, the second border collision of the 5-cycle can be determined by solving for $T_{\mathrm{R}}^4 \circ T_{\mathrm{L}}\,(x, y) = (x, y)$ and then considering $y = 0$.

Similarly, we can reason for any cycle with symbolic sequence LR^n, for $n \geq 2$. So one BCB is obtained solving for $T_{\mathrm{L}} \circ T_{\mathrm{R}}^n\,(x, y) = (x, y)$ and then considering $y = 0$, and the other from $T_{\mathrm{R}}^n \circ T_{\mathrm{L}}\,(x, y) = (x, y)$ and then considering $y = 0$.

It follows that in order to obtain a period point and the BCB conditions for cycles with symbolic sequence LR^n, we have to consider a fixed point of the composite function $T_{\mathrm{L}} \circ T_{\mathrm{R}}^n\,(x, y)$ or $T_{\mathrm{R}}^n \circ T_{\mathrm{L}}\,(x, y)$ which requires, in particular, the function $T_{\mathrm{R}}^n\,(x, y)$ which is not easy to get for an affine function as we have in map T. Clearly, it is much easier with a linear function such as $\widetilde{T}_{\mathrm{R}}\,(x, y) = A_{\mathrm{R}} \begin{pmatrix} x \\ y \end{pmatrix}$ where $A_{\mathrm{R}} = \begin{bmatrix} t_{\mathrm{R}} & -d_{\mathrm{R}} \\ 1 & 0 \end{bmatrix}$. In fact, in such a linear case the composition $\widetilde{T}_{\mathrm{R}}^n\,(x, y) = A_{\mathrm{R}}^n \begin{pmatrix} x \\ y \end{pmatrix}$ can be obtained iteratively (thus in a easier way). It is well known (see, e.g., [45] and [21]) that we have

$$A_{\mathrm{R}}^n = \begin{bmatrix} a_n & -d_{\mathrm{R}} a_{n-1} \\ a_{n-1} & -d_{\mathrm{R}} a_{n-2} \end{bmatrix}, \text{ for } n \geq 2 \tag{33}$$

where the constants are obtained iteratively from

$$a_n = t_{\mathrm{R}} a_{n-1} - d_{\mathrm{R}} a_{n-2} \tag{34}$$

with initial conditions $a_0 = 1$ and $a_1 = t_{\mathrm{R}}$. Thus, in order to take advantage of this formulation, since our maps are affine and not linear, we have first to apply a change of variable putting the origin in the point $P_{\mathrm{R}}^* = \left(x_{\mathrm{R}}^*, x_{\mathrm{R}}^*\right)$, that is, by applying the change of variable $(u, v) = \left(x - x_{\mathrm{R}}^*, y - x_{\mathrm{R}}^*\right)$ to the two components of map T. The new map $\widetilde{T}\,(u, v)$ is defined as follows:

$$\widetilde{T}\begin{pmatrix} u \\ v \end{pmatrix} = \begin{cases} \widetilde{T}_{\mathrm{R}}(u, v_t) = \begin{pmatrix} t_{\mathrm{R}} & -d_{\mathrm{R}} \\ 1 & 0 \end{pmatrix} \begin{pmatrix} u \\ v \end{pmatrix} & \text{if } u > -x_{\mathrm{R}}^* \\ \widetilde{T}_{\mathrm{L}}(u, v) = \begin{pmatrix} t_{\mathrm{L}} & -d_{\mathrm{L}} \\ 1 & 0 \end{pmatrix} \begin{pmatrix} u \\ v \end{pmatrix} + \begin{pmatrix} m_{\mathrm{L}}(1 - \frac{x_{\mathrm{R}}^*}{x_{\mathrm{L}}^*}) \\ 0 \end{pmatrix} & \text{if } u < -x_{\mathrm{R}}^* \end{cases} \tag{35}$$

or equivalently as

$$\widetilde{T}\begin{pmatrix} u \\ v \end{pmatrix} = \begin{cases} \widetilde{T}_{\mathrm{R}}(u, v_t) = A_{\mathrm{R}} \begin{pmatrix} u \\ v \end{pmatrix} & \text{if } u > -x_{\mathrm{R}}^* \\ \widetilde{T}_{\mathrm{L}}(u, v) = A_{\mathrm{L}} \begin{pmatrix} u \\ v \end{pmatrix} + \begin{pmatrix} m_{\mathrm{L}}(1 - \frac{x_{\mathrm{R}}^*}{x_{\mathrm{L}}^*}) \\ 0 \end{pmatrix} & \text{if } u < -x_{\mathrm{R}}^* \end{cases} \tag{36}$$

where we underline that

$$\begin{aligned} m_{\mathrm{L}}(1 - \frac{x_{\mathrm{R}}^*}{x_{\mathrm{L}}^*}) &= x_{\mathrm{R}}^* (\frac{m_{\mathrm{L}}}{m_{\mathrm{R}}}(1 - t_{\mathrm{R}} + d_{\mathrm{R}}) - (1 - t_{\mathrm{L}} + d_{\mathrm{L}})) \\ &= x_{\mathrm{R}}^* \left(-\frac{m_{\mathrm{L}}}{m_{\mathrm{R}}} s_{\mathrm{R}} + s_{\mathrm{L}} \right) \end{aligned} \tag{37}$$

From our reasoning above, we have that for a $(n+1)$-cycle with symbolic sequence $\mathrm{LR}^n, n \geq 2$, one BCB condition can be obtained looking for a periodic point (u, v) such that $\widetilde{T}_{\mathrm{L}} \circ \widetilde{T}_{\mathrm{R}}^n (u, v) = (u, v)$ leading to the system

$$\begin{pmatrix} t_{\mathrm{L}}(a_n u - d_{\mathrm{R}} a_{n-1} v) - d_{\mathrm{L}}(a_{n-1} u - d_{\mathrm{R}} a_{n-2} v) + m_{\mathrm{L}}(1 - \frac{x_{\mathrm{R}}^*}{x_{\mathrm{L}}^*}) \\ a_n u - d_{\mathrm{R}} a_{n-1} v \end{pmatrix} = \begin{pmatrix} u \\ v \end{pmatrix} \tag{38}$$

and then a collision occurs when $y = 0$ corresponding to $v = -x_{\mathrm{R}}^*$, from which we obtain the following condition on the parameters:

$$\begin{aligned} &\frac{m_{\mathrm{L}}}{m_{\mathrm{R}}}(1 - t_{\mathrm{R}} + d_{\mathrm{R}}) - (1 - t_{\mathrm{L}} + d_{\mathrm{L}}) \\ &\quad = -\frac{(1 + d_{\mathrm{R}} a_{n-1})(1 - t_{\mathrm{L}} a_n + d_{\mathrm{L}} a_{n-1})}{a_n} \\ &\qquad - t_{\mathrm{L}} d_{\mathrm{R}} a_{n-1} + d_{\mathrm{L}} d_{\mathrm{R}} a_{n-2} \end{aligned} \tag{39}$$

The second BCB involving this cycle is identified by another BCB condition which is obtained looking for a periodic point (u, v) such that $\widetilde{T}_{\mathrm{R}}^n \circ \widetilde{T}_{\mathrm{L}} (u, v) = (u, v)$ leading to the system

$$\begin{pmatrix} a_n(t_{\mathrm{L}} u - d_{\mathrm{R}} v + m_{\mathrm{L}}(1 - \frac{x_{\mathrm{R}}^*}{x_{\mathrm{L}}^*})) - d_{\mathrm{R}} a_{n-1} u \\ a_{n-1}(t_{\mathrm{L}} u - d_{\mathrm{R}} v + m_{\mathrm{L}}(1 - \frac{x_{\mathrm{R}}^*}{x_{\mathrm{L}}^*})) - d_{\mathrm{R}} a_{n-2} v \end{pmatrix} = \begin{pmatrix} u \\ v \end{pmatrix} \tag{40}$$

and then a collision occurs when $y = 0$ corresponding to $v = -x_{\mathrm{R}}^*$, from which we obtain the following condition on the parameters:

$$\begin{aligned} &\frac{m_{\mathrm{L}}}{m_{\mathrm{R}}}(1 - t_{\mathrm{R}} + d_{\mathrm{R}}) - (1 - t_{\mathrm{L}} + d_{\mathrm{L}}) \\ &\quad = -\frac{(1 + d_{\mathrm{L}} a_{n-1})(1 - t_{\mathrm{L}} a_n + d_{\mathrm{R}} a_{n-1}) + d_{\mathrm{L}} a_n (a_{n-1} t_{\mathrm{L}} - d_{\mathrm{R}} a_{n-2})}{a_n (a_{n-1} t_{\mathrm{L}} - d_{\mathrm{R}} a_{n-2}) + a_{n-1}(1 - a_n t_{\mathrm{L}} + d_{\mathrm{R}} a_{n-1})} \end{aligned} \tag{41}$$

A few existing regions Π_{LR^n} of the cycles LR^n, $n = 2, 3, 4$ are shown in Fig. 4 at the parameters given in (24), in red those given in (39) and in black those given in (41). We can see that the regions Π_{LR^2} and Π_{LR^3} are overlapping, as also the regions Π_{LR^3} and Π_{LR^4} are overlapping. The overlapped regions indicate the coexistence of multiple attractors.

It is plain that we can reason similarly to obtain the existence conditions for the basic $(n+1)$-cycles with symbolic sequence RL^n, $n \geq 2$. However, due to the symmetry between the two functions T_{L} and T_{R} with respect to the symbols L/R, to get the conditions for the other family of basic cycles it is enough to exchange L/R in the expressions given above, that is, by using, for $n \geq 2$

$$\overline{a}_n = t_{\mathrm{L}} \overline{a}_{n-1} - d_{\mathrm{L}} \overline{a}_{n-2} \tag{42}$$

with initial conditions $\overline{a}_0 = 1$ and $\overline{a}_1 = t_{\mathrm{L}}$, we have

$$\begin{aligned} &\frac{m_{\mathrm{R}}}{m_{\mathrm{L}}}(1 - t_{\mathrm{L}} + d_{\mathrm{L}}) - (1 - t_{\mathrm{R}} + d_{\mathrm{R}}) \\ &\quad = -\frac{(1 + d_{\mathrm{L}} \overline{a}_{n-1})(1 - t_{\mathrm{R}} \overline{a}_n + d_{\mathrm{R}} \overline{a}_{n-1})}{\overline{a}_n} \\ &\qquad - t_{\mathrm{R}} d_{\mathrm{L}} \overline{a}_{n-1} + d_{\mathrm{L}} d_{\mathrm{R}} \overline{a}_{n-2} \end{aligned} \tag{43}$$

and

$$\begin{aligned} &\frac{m_{\mathrm{R}}}{m_{\mathrm{L}}}(1 - t_{\mathrm{L}} + d_{\mathrm{L}}) - (1 - t_{\mathrm{R}} + d_{\mathrm{R}}) \\ &\quad = -\frac{(1 + d_{\mathrm{R}} \overline{a}_{n-1})(1 - t_{\mathrm{R}} \overline{a}_n + d_{\mathrm{L}} \overline{a}_{n-1}) + d_{\mathrm{R}} \overline{a}_n (\overline{a}_{n-1} t_{\mathrm{R}} - d_{\mathrm{L}} \overline{a}_{n-2})}{\overline{a}_n (\overline{a}_{n-1} t_{\mathrm{R}} - d_{\mathrm{L}} \overline{a}_{n-2}) + \overline{a}_{n-1}(1 - \overline{a}_n t_{\mathrm{R}} + d_{\mathrm{L}} \overline{a}_{n-1})} \end{aligned} \tag{44}$$

A few existing regions of the cycles RL^n, $n = 2, \ldots, 5$ are shown in Fig. 4, in red those given in (43) and in black those given in (44). We can see that the regions Π_{LR^n} and $\Pi_{\mathrm{LR}^{n+1}}$ for $n = 2, 3, 4$ are overlapping.

Besides the existence of some regions of the basic cycles of the two families LR^n and RL^n, we can evidence that between two consecutive existing regions of cycles LR^n and LR^{n+1} it may exist a region associated with a cycle with symbolic sequence obtained by concatenation, $\mathrm{LR}^n\mathrm{LR}^{n+1}$. However, while in the discontinuous one-dimensional case such regions cannot overlap ([4,22] and references therein) and are all disjoint, in our map we have seen (in the example above) that regions of the basic cycles of the two families LR^n and RL^n may overlap, and when these are disjoint, it is quite common that when a cycle with symbolic sequence obtained by concatenation, say $\mathrm{LR}^n\mathrm{LR}^{n+1}$, exists, then this region is overlapped with the regions of the two basic cycles. As an example, in Fig. 4a, between the regions associated with the cycles LR and RL^2 a region related to a 5-cycle with symbolic sequence LRLR^2 exists, and it is overlapped with both the regions of the cycles LR and LR^2. Similarly for the other family: between the regions associated with the cycles RL and RL^2 a region related to a 5-cycle with symbolic sequence RLRL^2 exists, and it is overlapped with both the regions of the cycles RL and RL^2. It is worth mentioning that between non-overlapping regions of basic cycles with symbolic sequences LR^n and LR^{n+1} the region related to the cycle with the 'concatenated' symbolic sequence $\mathrm{LR}^n\mathrm{LR}^{n+1}$ exists, and in general it is not overlapped with the regions of the basic cycles. Indeed, many regions of cycles with the

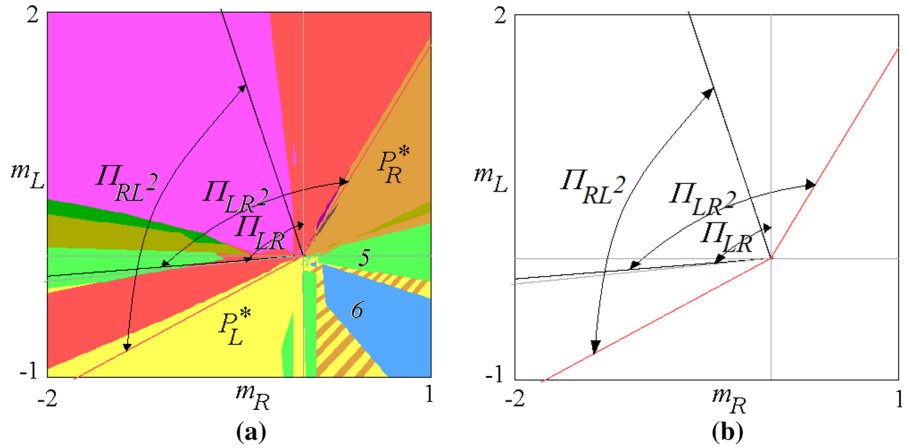

Fig. 6 Two-dimensional bifurcation diagram of the map T with respect to the parameter plane (m_R, m_L). The straight lines coming out of the origin are the border collision bifurcation curves and mark the regions of cycles, with symbolic sequence LR, LR^2 and RL^2. Parameters: $d_L = 0.8$, $s_L = -2$, $d_R = 0.9$ and $s_R = -2$. The meaning of the colors is shown in Fig. 4

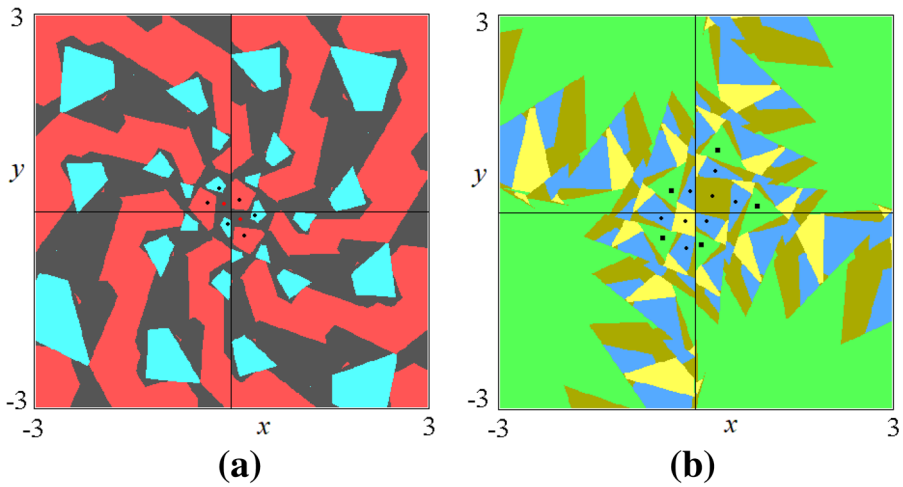

Fig. 7 Graphic representation of the subregion $(-3, 3)\times(-3, 3)$ of the phase space of the map T. The brown region represents the basin of attraction of the 2-period cycle with symbolic sequence LR, the cyan region represents the basin of attraction of a 3-period cycle with symbolic sequence RL^2, the red region represents the basin of attraction of a 3-period cycle with symbolic sequence LR^2, the yellow region represents the basin of attraction of the bear market equilibrium (x_L^*, y_L^*), the corn region represents the basin of attraction of the bull market equilibrium (x_R^*, y_R^*), the blue region represents the basin of attraction of a 6-period cycle with symbolic sequence R^3L^3, and the green region represents the basin of attraction of a 5-period cycle with symbolic sequence L^2R^3. Panel (**a**) $m_R = -0.2$ and $m_L = 0.2$. Panel (**b**) $m_R = 0.5$ and $m_L = -0.3$. The parameters d_L, s_L, d_R and s_R are shown in Fig. 6, i.e., $d_L = 0.8$, $s_L = -2$, $d_R = 0.9$ and $s_R = -2$

symbolic sequence $(LR^n)^m LR^{n+1}$ and $LR^n(LR^{n+1})$ for $m > 1$, of the second complexity level may also exist disjoint, between the regions of the basic cycles, as well as regions corresponding to cycles of higher complexity level. Similarly for the other family with symbolic sequences RL^n and RL^{n+1}. For the sake of space, we do not show numerically such possible situations.

A peculiarity of our two-dimensional discontinuous PWL map is also that when the two fixed points coexist and are attracting, then these may coexist with other attracting cycles. An example is shown in Fig. 6, where a two-dimensional bifurcation diagram of the map T with respect to the parameter plane (m_R, m_L) is obtained by setting $d_L = 0.8$, $s_L = -2$ (so that $t_L = -0.2$) and $d_R = 0.9$, $s_R = -2$ (so that $t_L = -0.1$). Here, cycles with symbolic sequences RL, LR^2 and RL^2 are overlapped when the two fixed points are virtual (an example in the phase space is shown in Fig. 7a at $m_R = -0.2$ and $m_L = 0.2$), but attracting

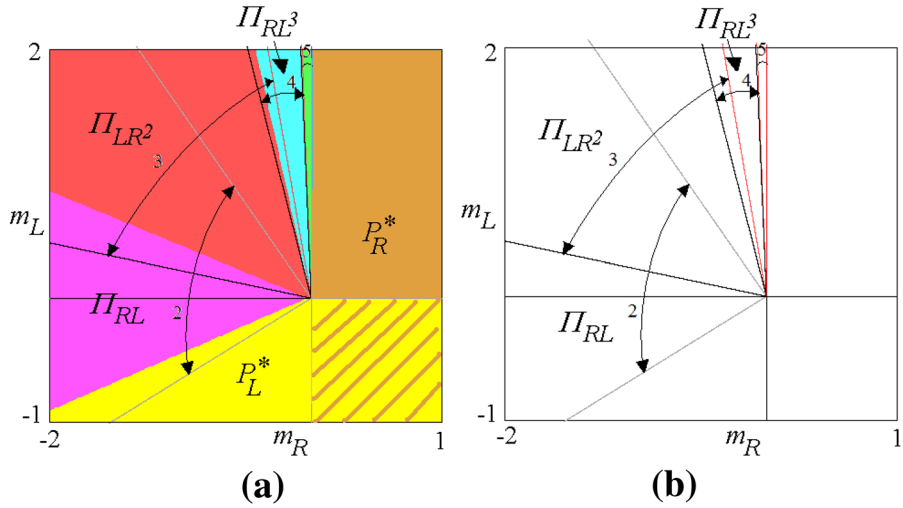

Fig. 8 Two-dimensional bifurcation diagram of the map T with respect to the parameter plane $(m_{\mathrm{R}}, m_{\mathrm{L}})$. The straight lines coming out of the origin are the border collision bifurcation curves and mark the regions of cycles, with symbolic sequence LR, LR^2 and RL^2. Parameters: $d_{\mathrm{L}} = 0.03$, $s_{\mathrm{L}} = -1.8$, $d_{\mathrm{R}} = 0.18$ and $s_{\mathrm{R}} = -0.5$. The meaning of the colors is shown in Fig. 4

cycles of period 5 and 6 may also exist when both fixed points are real and attracting (an example in the phase space is shown in Fig. 7b at $m_{\mathrm{R}} = 0.5$ and $m_{\mathrm{L}} = -0.3$).

As a further remark, we may also expect that the bifurcation structure in the $(m_{\mathrm{R}}, m_{\mathrm{L}})$ parameter plane changes when the two fixed points have different eigenvalues. An example is given at $d_{\mathrm{L}} = 0.03$, $s_{\mathrm{L}} = -1.8$ (so that $t_{\mathrm{L}} = -0.77$) and the fixed point in the left region is an attracting node with two negative eigenvalues, while $d_{\mathrm{R}} = 0.18$, $s_{\mathrm{R}} = -0.5$ (so that $t_{\mathrm{L}} = 0.68$) and the fixed point on the right side is an attracting focus, see Fig. 8. We can observe that now only cycles of the family LR^n are attracting when the two fixed points are virtual; moreover, the real attracting fixed point P_{R}^* may coexist with an attracting 5-cycle while the real attracting fixed point P_{L}^* may coexist with an attracting 2-cycle.

4 Chaotic dynamics in the deterministic setting

As it is well known, it is not surprising to have a two-dimensional invertible map with chaotic behaviors. This is clearly possible in continuous maps as well as in discontinuous ones, as we are considering in this work. Up to now, we have mentioned mainly regimes with coexisting attracting cycles of different periods, but such attracting cycles may also coexist with chaotic attractors. This is also another important difference between the one-dimensional discontinuous map and the two-dimensional one. In fact, considering for example the one-dimensional map

$$x_{t+1} = \begin{cases} \tau_{\mathrm{R}} x_t + m_{\mathrm{R}} & \text{if } x_t > 0 \\ \tau_{\mathrm{L}} x_t + m_{\mathrm{L}} & \text{if } x_t < 0 \end{cases} \tag{45}$$

in the increasing–increasing case given by positive slopes $(\tau_{\mathrm{R}}, \tau_{\mathrm{L}})$ and $m_{\mathrm{R}} < 0$, $m_{\mathrm{L}} > 0$, it is well known that as long as $\tau_{\mathrm{R}} m_{\mathrm{L}} + m_{\mathrm{R}} < \tau_{\mathrm{L}} m_{\mathrm{R}} + m_{\mathrm{L}}$, which is the so-called gap map, then chaotic dynamics cannot occur, as well as for the circle map occurring when $\tau_{\mathrm{R}} m_{\mathrm{L}} + m_{\mathrm{R}} = \tau_{\mathrm{L}} m_{\mathrm{R}} + m_{\mathrm{L}}$, see Avrutin et al. [4] and references therein. Clearly chaos can exist when the map is overlapping, that is, it becomes not uniquely invertible. Differently, in the two-dimensional case we may have chaotic regimes also when the map is invertible, as in the cases here considered (with $d_{\mathrm{R}} > 0$ and $d_{\mathrm{L}} > 0$) and also when both determinants d_{R} and d_{L} are smaller than 1, so that the map cannot have expanding cycles (as repelling nodes or foci), but only saddle cycles which may be homoclinic, leading to chaotic dynamics. To provide an immediate visualization of the dynamics which may emerge, in Fig. 9 we show a two-dimensional bifurcation diagram in the $(s_{\mathrm{R}}, s_{\mathrm{L}})$ parameter plane at fixed $0 < d_{\mathrm{R}} < 1$, $0 < d_{\mathrm{L}} < 1$, $m_{\mathrm{R}} < 0$ and $m_{\mathrm{L}} > 0$ (similar figures are obtained at different parameter values). In Fig. 9a, different colors represent periodicity regions associated with attracting cycles of different periods. Several regions Π_{LR^n} and Π_{RL^n} bounded by BCB curves whose equations are given in Sect. 3 are clearly visible, and it is also clearly visible that many of such regions are overlapping. The white points denote the existence of chaotic dynamics, while the gray points denote the existence of divergent trajectories. A relevant feature in this kind of

systems, piecewise linear, which usually cannot occur in smooth ones, is that when chaotic attractors exist (and mainly appearing/disappearing via BCBs), they are stable under parameter perturbations, that is, they are *robust*, following the definition given in Banerjee et al. [5].

One-dimensional bifurcation diagrams along the three paths denoted by p_1, p_2 and p_3 in Fig. 9a are shown in Fig. 9b, Fig. 9c and Fig. 9d, respectively. The diagrams have been drawn with three different initial conditions and the x-values are reported in different colors (black, red and azure), so as to emphasize parameter value constellations associated with coexisting attracting sets.

The path p_1 is taken along the line $s_R = s_L$, and regular periodicity regions are crossed as long as $s_R = s_L < 0$ (when the two fixed points are both virtual and mainly attracting), while for $s_R = s_L > 0$ the two fixed points, crossing the bifurcation occurring at $s_R = 0$ and $s_L = 0$, become real and of saddle type, with one positive eigenvalue larger than 1, and chaotic dynamics occur. An example in the phase plane of the chaotic attracting set for $s_R > 0$ and $s_L > 0$, corresponding to point A_1 in Fig. 9a, is shown in Fig. 10a. The two stable sets of the saddle fixed points belong to the basin boundary of the chaotic attracting set, together with segments of the discontinuity line $x = 0$ (and related preimages). The basin boundary separates points with bounded trajectories from those having divergent trajectories.

Differently, when the parameters s_R and s_L have different signs, then one fixed point is real and one is virtual. When the virtual one is attracting then, even if the real fixed point with positive parameter s is a saddle with one eigenvalue larger than 1, bounded chaotic dynamics are observed. An example is shown in Fig. 10b, corresponding to point A_2 in Fig. 9a, where $P_L^* = (1, 1)$ is a virtual attracting focus, while P_R^* is a real saddle, whose stable set belongs to the basin boundary of the chaotic attracting set (together with segments of the discontinuity line $x = 0$ and related preimages).

Also when both fixed points are virtual and attracting, besides periodicity regions associated with attracting cycles, we may have chaotic attractors, as unique attracting sets or coexisting with attracting cycles. An example is shown in Fig. 10c, corresponding to point A_3 in Fig. 9a, where $P_L^* = (1, 1)$ and $P_R^* = (-0.4, -0.4)$ are both virtual attracting foci, and the chaotic attractor (with basin colored in red) coexists with an attracting 11-cycle, three periodic points of which are visible in Fig. 10c. The two basins are here separated only by segments of the discontinuity line $x = 0$ and related preimages.

5 Stochastic dynamics of the asset pricing model

In the previous two sections, a description of the dynamics of the deterministic setting of the model is proposed. In this section, we exploit these results to replicate the statistical properties of the returns of the financial markets with the stochastic version of our model. To this aim, let us start underlining the main properties of the time series of the returns of market indexes. Focusing on the daily observations of the value of the S&P 500 index over the last twenty years, see Fig. 11a, we observe that the related returns show periods of high volatility alternated by periods of low volatility, see Fig. 11c. Specifically, during the 2007 financial crisis we observe a persistent period of high volatility that is followed by a long period of low volatility. Periods of high volatility followed by periods of low volatility are a *stylized fact* known in the financial literature as *volatility clustering*. The statistical confirmation of the volatility clustering effect is given by the sample autocorrelation functions that show a statistically significant long correlation in the squared returns and absolute returns, while the almost zero correlation in the returns supporting the classical hypotheses of the random walk models, see Fig. 11d–f. The volatility clustering effect reflects in an empirical distribution of the returns that is not normal, see Fig. 11c. Indeed, the empirical distribution of the returns is usually skewed to the left, see the negative skewness in Table 1, with extreme returns that are more often than in a normal distribution as indicated by the presence of the so-called heavy tails or fat tails. The *tailedness* of the empirical distribution of the returns is measured by the sample kurtosis, which is around 11, therefore much higher than the value 3 which characterizes a normal distribution. This indicates that the distribution of the returns is *leptokurtic*, i.e., it has heavy tails. See Table 1.

The asset pricing models with heterogeneous agents aim to replicate these features of the distribution of the returns. In particular, they aim to explain the nonlinear dependence in the returns, which indicates the pres-

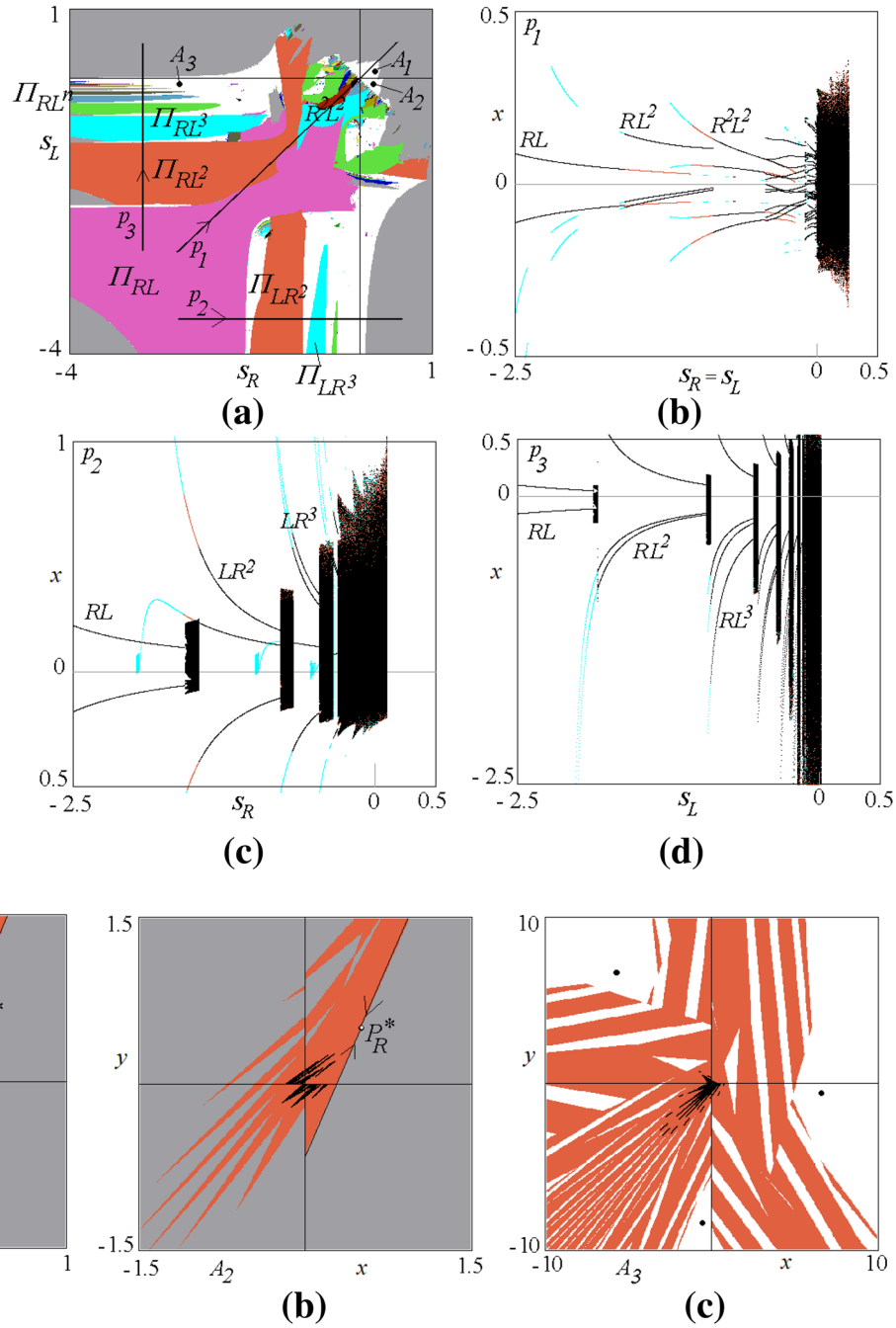

Fig. 9 In Panel (**a**), two-dimensional bifurcation diagram in the (s_R, s_L) parameter plane at $d_R = 0.6$, $d_L = 0.9$, $m_R = -0.1$ and $m_L = 0.1$ (similar figures are obtained at different parameter values). In Panel (**b**), one-dimensional bifurcation diagram along the path denoted by p_1 in Panel (**a**), and $s_R = s_L$. In Panel (**c**), one-dimensional bifurcation diagram along the path denoted by p_2 in Panel (**a**), and $s_L = -3.5$. In Panel (**d**), one-dimensional bifurcation diagram along the path denoted by p_3 in Panel (**a**), and $s_R = -3$

Fig. 10 Chaotic attracting sets and related basins of attraction (in red) at $d_R = 0.6$, $d_L = 0.9$, $m_R = -0.1$, $m_L = 0.1$. Gray points denote initial conditions leading to divergent trajectories. In Panel (**a**) $(s_R, s_L) = (0.25, 0.1)$, point A_1 in Fig. 9a, so that $t_R = 1.85$, $t_L = 2$, the two fixed points are real saddles ($P_L^* = (-1, -1)$, with $\lambda_1 = 1.316$ and $\lambda_2 = 0.684$, $P_R^* = (0.4, 0.4)$ with $\lambda_1 = 1.43$ and $\lambda_2 = 0.42$) with the stable sets belonging to the basin boundary, and the immediate stable set of each fixed point, the eigenvector given in (19), is also evidenced. In Panel (**b**) $(s_R, s_L) = (0.2, -0.1)$, point A_2 in Fig. 9a, so that $t_R = t_L = 1.8$, $P_L^* = (1, 1)$ is a virtual attracting focus, $P_R^* = (0.5, 0.5)$ a real saddle with $\lambda_1 = 1.358$ and $\lambda_2 = 0.44$, the immediate stable set is also evidenced. In Panel (**c**) $(s_R, s_L) = (-2.5, -0.1)$, point A_3 in Fig. 9a, so that $t_R = -0.9$, $t_L = 1.8$, $P_L^* = (1, 1)$ and $P_R^* = (-0.04, -0.04)$ are virtual foci

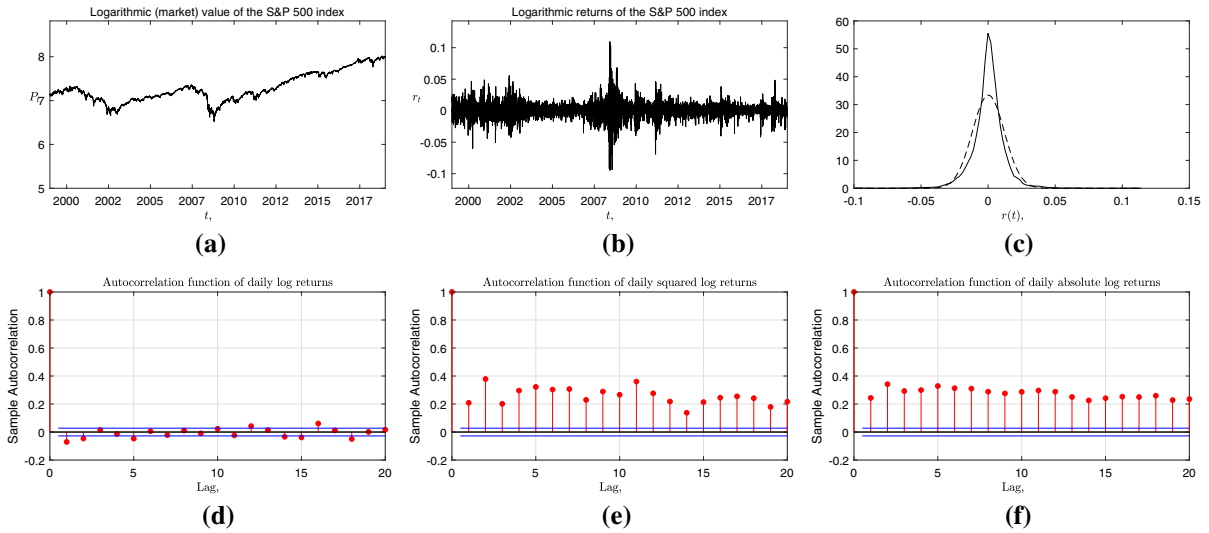

Fig. 11 Panel (**a**) dynamics of logarithmic value of the day by day S&P 500 index over the period 1/1/1999–1/10/2019. Panel (**b**) time series of the logarithmic daily returns of the S&P 500 index for the period 1/1/1999–1/10/2019. Panel (**c**) the solid line represents the empirical distribution of the logarithmic returns of the S&P 500 index, while the dashed line represents the calibrated normal distribution, where the calibration is obtained by using the daily returns of the S&P 500 index. Panel (**d**) autocorrelation function of the logarithmic daily returns of the S&P 500 index. Panel (**e**) behavior of the correlation function of the square of the logarithmic daily returns of the S&P 500 index. Panel (**f**) behavior of the correlation function of the absolute value of the logarithmic daily returns of the S&P 500 index. The data source is Thomson Reuters Eikon

Table 1 Statistics related to the S&P 500 index returns, see also Fig. 11

Statistics	Average	Min	Max	Volatility	Skewness	Kurtosis
S&P 500 index returns	0.0002	−0.0947	0.1096	0.0119	−0.2127	11.2181

ence of the volatility clustering effect, by a quantitative point of view, see He and Li [26] and Blaurock et al. [7]. Parsimonious asset pricing models as the one here considered have the further advantage to provide also a qualitative explanation for the stylized facts of the empirical distributions of the returns of stocks, commodities and market indexes. Considering the deterministic skeleton of a model as indicated in Gaunersdorfer et al. [23], the coexistence of a stable equilibrium surrounded by a stable cycle represents a qualitative and endogenous explanation for the volatility clustering effect. In fact, forcing the dynamics of the model by a stochastic noise, prices jump from the basin of attraction of the equilibrium where returns are characterized by low volatility, to the basin of attraction of the cycle, where returns are characterized by high volatility. The deterministic investigation of the model in the previous section indicates that a similar configuration of the dynamics is present in the asset pricing model here considered. Specifically, a stable equilibrium can coexist with a stable cycle. According to the parameter value configuration, it could be the bear market equilibrium that coexists with a cycle or it could be the bull market equilibrium that coexists with a cycle. Moreover, a chaotic attractor can coexist with a cycle. It is worth remarking that the coexistence of several attractors is related to the presence of the trend followers. In fact, excluding the trend followers from our asset pricing model, we are back in the setup introduced in Tramontana et al. [47] where a stable equilibrium cannot coexist with a stable periodic, aperiodic or chaotic attractor. Therefore, the introduction of the trend followers gives to the current generalization of the asset pricing model in Tramontana et al. [47] the advantage of offering a qualitative configuration of the dynamics that is associated with the volatility clustering effect.

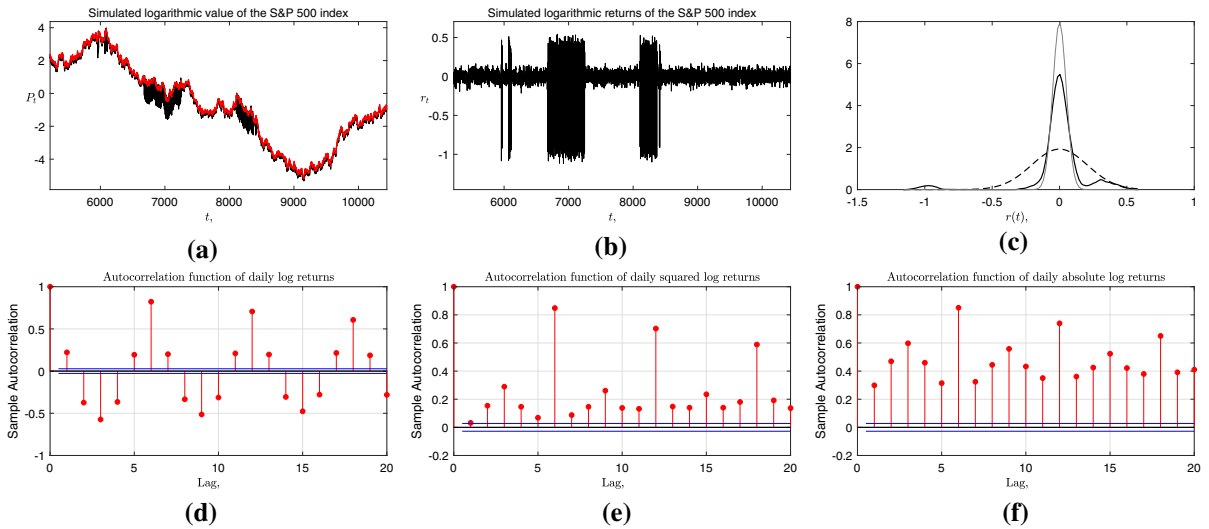

Fig. 12 Results are obtained by simulating the asset pricing model (8) under constellation of parameter values as shown in (24) with $m_{\mathrm{L}} = -0.05$, $m_{\mathrm{R}} = -1$ and $\sigma_F = 0.05$. Panel (**a**) in red is represented the dynamics of the fundamental process defined in (1) while in black the price of the asset generated by model (8). Panel (**b**) logarithmic returns related to the price dynamics (in black) of Panel (**a**). Panel (**c**) simulated distribution of the returns (solid line), normal distribution calibrated to the simulated returns (dashed line) and normal distribution used to generate the fundamental price (gray line). Panel (**d**) autocorrelation function for the logarithmic returns in Panel (**b**). Panel (**e**) autocorrelation function for the square of the logarithmic returns in Panel (**b**). Panel (**f**) autocorrelation function for the absolute value of the logarithmic returns in Panel (**b**). Statistics related to the simulated distribution of the logarithmic returns are shown in Table 2

Table 2 Statistics related to the returns obtained by simulating the asset pricing model (8) (and the random walk fundamental process) under constellation of parameter values as shown in (24) with $m_{\mathrm{L}} = -0.05$, $m_{\mathrm{R}} = -1$ and $\sigma_F = 0.05$, see also Fig. 12

Statistics	Average	Min	Max	Volatility	Skewness	Kurtosis
Asset pricing model	− 0.0006	− 1.1173	0.5425	0.2070	− 2.6697	15.7476
Fundamental process	− 0.0006	− 0.1967	0.1695	0.0499	− 0.0040	2.9976

To analyze the characteristics of the time series of the returns generated by the full-fledged stochastic version of our model, we assume the set of parameter values as shown in (24) with $m_{\mathrm{L}} = -0.05$, $m_{\mathrm{R}} = -1$ and $\sigma_F = 0.05$. This parameter value configuration is associated with a deterministic dynamics characterized by a stable bear market equilibrium P_{L}^* coexisting with a stable 6-period cycle, see Fig. 3b. Introducing some noise, see Fig. 12, we observe that the time series of the returns show periods of high volatility alternated by periods of low volatility. Moreover, comparing Table 1 with Table 2, we observe that the simulated distribution of the returns is not normal and has a level of kurtosis similar to the one of the empirical distribution, while the skewness indicates that the simulated distribution is much more left-skewed than the empirical one and both of these two values of the skewness are different from one of the normal distributions. In addition, we observe that the returns generated by our asset pricing model are much more volatile than the returns generated by the fundamental random walk process, see Table 2. This stylized fact is known as *excess volatility*.

Despite some analogies between the empirical and simulated distributions of the returns, the presence of a stable 6-period cycle introduces a deterministic structure in the dynamics of the returns, which mirrors in a dependence in the returns that is not observable in the empirical data, see Fig. 11d. This is indicated by the autocorrelation function of the returns that underlines a statistically significant correlation, see Fig. 12d. A qualitative configuration of the dynamics where an aperiodic or chaotic attractor coexists with a stable equi-

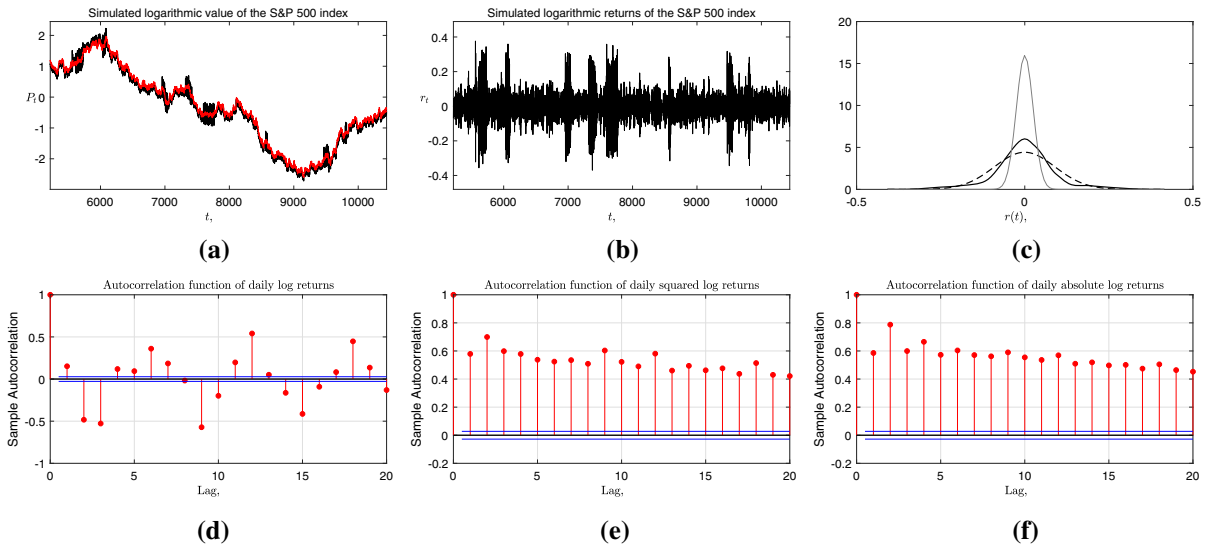

Fig. 13 Results are obtained by simulating the asset pricing model (8) under constellation of parameter values as in Fig. 7a, but $\sigma_F = 0.025$. The meaning of the graphs is shown in Fig. 12. Statistics related to the simulated distribution of the logarithmic returns are shown in Table 3

librium would probably reduce the level of correlation in the returns, therefore obtaining a dynamics of the returns more similar to the empirical one.

The simulated time series of the returns show also that the periods of high volatility have a frequency of occurrence higher than that one suggested by the empirical observations. This may depend on the configuration of the basins of attraction, that for the deterministic version of the model result to be disconnected and intermingled, see Fig. 3b, thus facilitating a frequent and sudden transition from one (characterized by low volatility) to the other attractor (characterized by high volatility) when some random noise is added to the system. Another relevant difference between the simulated dynamics of the returns and the empirical one is the magnitude of the returns itself that in the simulated model are much higher than the observed one. To overcome this problem, it is enough to focus on a constellation of the values of the parameters such that the deterministic skeleton of the model shows long-run dynamics characterized by lower amplitude fluctuations. An example is given in Fig. 3c. However, in the dynamic configuration depicted in Fig. 3c only cyclical attractors exist, specifically a 2-period cycle and a 4-period cycle while a stable equilibrium misses, and this reflects in a simulated distribution of the returns that is bimodal, therefore different from the empirical one.

In a configuration in which it is the bull market equilibrium, instead of the bear market equilibrium, that coexists with a cycle, see for example the case of Fig. 5a, a similar dynamics of the returns is obtained from the stochastic version of the model. Therefore, the simulated distribution of the returns differs from the empirical one for the reasons already discussed.

A further peculiarity of the asset pricing model here proposed is the coexistence of several attractors of different periodicities, see for example Fig. 7, which cannot occur in the one-dimensional version of the model proposed in Tramontana et al. [47]. To study the impact of this dynamic scenario on the distribution of the returns, consider the same set of values of the parameters as shown in Fig. 7a and $\sigma_F = 0.025$. The results of the simulation shown in Fig. 13 (in particular the dynamics of the logarithmic returns of the asset in Fig. 13b) underline the volatility clustering effect that is confirmed by the autocorrelation functions of the absolute and squared returns, see Fig. 13e, f. Moreover, compared with a normal distribution, the empirical distribution of the returns shows a greater concentration of observations around the average value and tails much fatter, see Fig. 13c. Skewness and kurtosis, see Table 3,

Table 3 Statistics related to the returns obtained by simulating the asset pricing model (8) (and the random walk fundamental process) under constellation of parameter values as in Fig. 7a, but $\sigma_F = 0.025$, see also Fig. 13

Statistics	Average	Min	Max	Volatility	Skewness	Kurtosis
Asset pricing model	− 0.0003	− 0.3694	0.3764	0.0902	− 2.6697	4.9230
Fundamental process	− 0.0003	− 0.0984	0.0848	0.0249	− 0.0040	2.9976

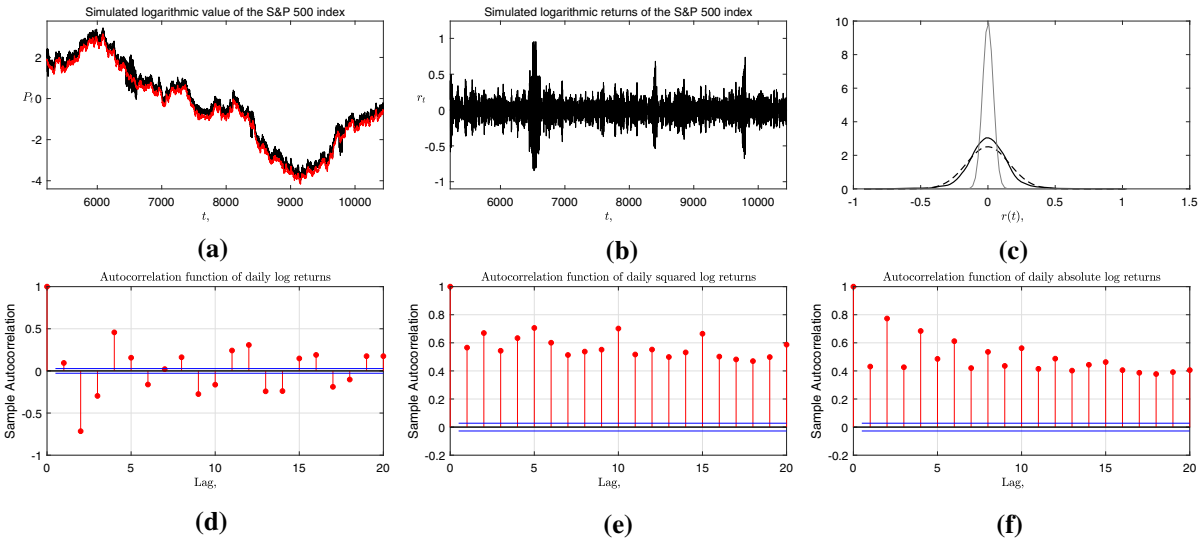

Fig. 14 Results are obtained by simulating the asset pricing model (8) under constellation of parameter values as in Fig. 7b, but $\sigma_F = 0.04$. The meaning of the graphs is shown in Fig. 12. Statistics related to the simulated distribution of the logarithmic returns are shown in Table 4

confirm these two facts and indicate that the simulated distribution of the returns is very similar to the empirical one. Again, the only feature of the simulated returns that does not match with the empirical observations is given by the correlation of the returns that in the simulated version is statistically significant while according to the real data it should not be so. As already indicated above, this is most probably due to the fact that we consider a constellation of the parameter values for which the deterministic skeleton of the asset pricing model exhibits periodic dynamics instead of chaotic dynamics.

A distribution of the returns similar to the empirical one can also be obtained by considering the value of the parameters as shown in Fig. 7b, but $\sigma_F = 0.04$. This is a particularly interesting configuration as the deterministic skeleton of the model offers three different volatility return regimes. Specifically, the stable bear market equilibrium is a configuration representing a level of return volatility equal to the one generated by the fundamental process, a stable 7-period cycle is responsible for a medium level of return volatility, and a stable 5-period cycle generates a high return volatility. The stochastic noise that affects the fundamental process allows to jump from one basin of attraction to another one causing periods of high volatility followed by periods of medium volatility, followed in turn by periods of low volatility. This dynamics generates an evident volatility clustering effect, see Fig. 14. Relevant is also the shape of the immediate basins of attraction, which being wide reduces the number of times that the noise causes a jump from one basin to another. Therefore, it increases the persistence of a volatility return regime. These features emphasize the volatility clustering effect. The simulated distribution of the returns has the usual properties already discussed, see Fig. 14c and Table 4.

Table 4 Statistics related to the returns obtained by simulating the asset pricing model (8) (and the random walk fundamental process) under constellation of parameter values as in Fig. 7b, but $\sigma_F = 0.04$, see also Fig. 14

Statistics	Average	Min	Max	Volatility	Skewness	Kurtosis
Asset pricing model	−0.0005	−0.8463	0.9552	0.1589	0.0979	7.3132
Fundamental process	−0.0005	−0.1574	0.1356	0.0399	−0.0040	2.9976

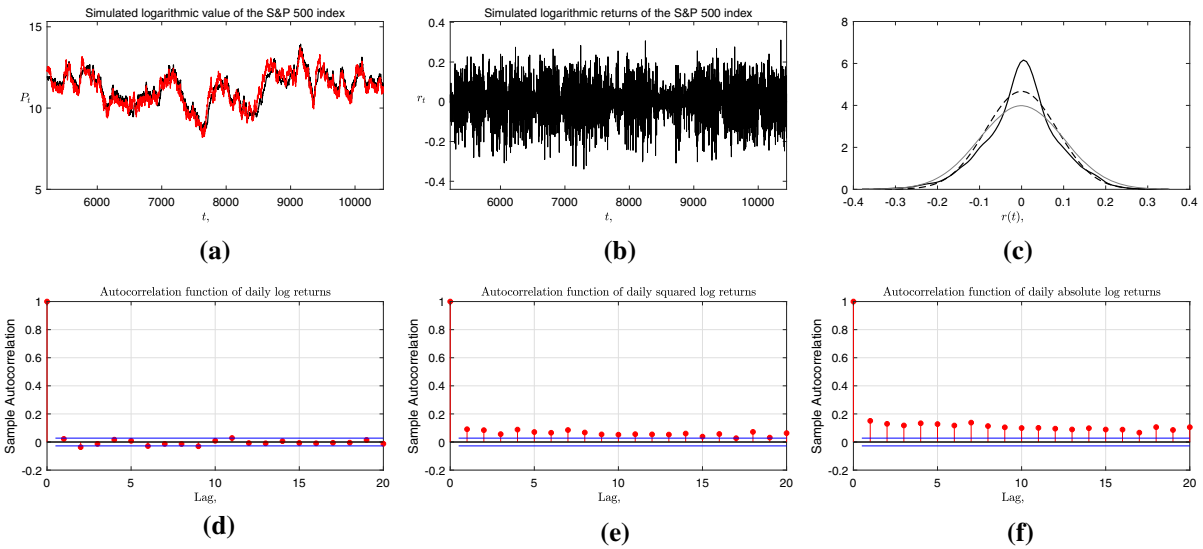

Fig. 15 Results are obtained by simulating the asset pricing model (8) under constellation of parameter values as follows, $d_R = 0.05$, $d_L = 0.08$, $s_R = -0.9$, $s_L = -0.05$, $m_R = 0.2$, $m_L = -0.02$, $\sigma_F = 0.1$. The meaning of the graph is shown in Fig. 12. Statistics related to the simulated distribution of the logarithmic returns are shown in Table 5

Table 5 Statistics related to the returns obtained by simulating the asset pricing model (8) (and the random walk fundamental process) under constellation of parameter values as follows, $d_R = 0.05$, $d_L = 0.08$, $s_R = -0.9$, $s_L = -0.05$, $m_R = 0.2$, $m_L = -0.02$, $\sigma_F = 0.1$, see also Fig. 15

Statistics	Average	Min	Max	Volatility	Skewness	Kurtosis
Asset pricing model	−0.0001	−0.3389	0.3107	0.0854	−0.2036	3.6961
Fundamental process	−0.0001	−0.3597	0.3421	0.0987	−0.0473	2.9338

The investigation so far conducted underlines that the distribution of the simulated returns is very sensitive to the configuration of the parameters and to the level of noise. A qualitative analysis of the deterministic skeleton of the model is therefore essential to identify the sets of parameter values such that multiple attractors exist and the volatility clustering effect can arise. Moreover, an ad hoc calibration of the level of noise is required to obtain a simulated distribution of the returns that resemble the empirical one. This underlines that it is also important to understand which ones are the dynamic configurations of the deterministic skeleton of an asset pricing model that allow to replicate stylized facts. Focusing again on the volatility clustering effect, we have already mentioned that the financial literature on models with heterogeneous expectations links this phenomenon to the coexistence of a stable limit cycle and a stable equilibrium (usually the fundamental equilibrium), as shown for example in Gaunersdorfer et al. [23], where the coexistence of a

stable steady state and a stable limit cycle occurs due to a so-called Chenciner bifurcation. Here, we have shown that the coexistence of a stable equilibrium and a cycle is also capable of generating the volatility clustering effect; however, the coexistence of multiple attractors occurs through border collision bifurcations instead of smooth bifurcations. It is also worth noting that since we have periodic orbits instead of limit cycles, we observe some autocorrelation in the returns, which is not observed in the empirical data. To overcome this drawback, we try to take a step forward by underlining a different configuration of the deterministic dynamics of the model that is associated with the volatility clustering phenomenon. Going back to the empirical data, see Fig. 11, we observe that the high volatility periods follow, or are sparked by, sharp drops in the price of an asset or in the value of a market index. See, for example, Fig. 11a, b. Moreover, being negative, the sample skewness indicates that the empirical distribution of the returns is left-tailed, i.e., extreme negative returns are more frequent than positive returns. Qualitative-wise, this phenomenon depends on the fact that asset prices (or index values) tend to rise slowly and to have drastic falls, causing extreme negative returns. This dynamics can be represented by a qualitative configuration of our model in which two equilibria coexist, a bear market equilibrium and a bull market equilibrium. The equilibrium that represents the bull market is stable (P_{R}^{*}) and has complex eigenvalues with real part that is close to zero, while the equilibrium that represents the bear market (P_{L}^{*}) is stable, but it has eigenvalues with real part almost equal to minus one. Therefore, the convergence to the bull market equilibrium is slow. At a qualitative level, we can imagine a situation in which the market slowly grows and converges to a stable bull market configuration. However, it may suffer some random fundamental shocks that force the price in a neighborhood of the equilibrium of the bear market. The switch between the bull market and the bear market occurs through a negative jump in the value of the asset which reflects in an extreme negative return. In the bear market, the negative eigenvalue of the bear market equilibrium indicates overshooting dynamics, with the price of the asset that jumps from above to below the bear market equilibrium. Therefore, positive and negative returns of large amplitude are recorded and a period of high volatile returns persists till the trajectory of prices goes back, forced by some random shock, to the bull market. In a bull market, low volatility is recorded. This configuration of the dynamics explains a possible mechanism through which the phenomenon of volatility clustering is generated. Moreover, this qualitative configuration of the dynamics is also able to replicate the so-called *rebound*, which means that a sudden and negative jump in the value of an asset is followed by another almost equally strong positive rebound. The stochastic dynamics of the model, see Fig. 15 and Table 5, confirms that such a deterministic configuration of the dynamics interplays with the fundamental random process to generate simulated data that replicate the empirical stylized facts, such as volatility clustering and fat tails. In addition, the autocorrelation function shows for the first time that the simulated returns are not statistically correlated.

The investigation conducted underlines how different configurations of the deterministic dynamics impact the simulated distribution of the returns. Moreover, the analysis is devoted to identify the deterministic dynamics that more often are associated with a specific stylized fact as it is the volatility clustering effect. In this respect, this contribution differs from the ones where a set of parameter values is identified via a trial-and-error calibration, or via a more sophisticated calibration procedure, to show a good match between the statistical properties of empirical and simulated data, see, e.g., Tramontana et al. [48].

6 Conclusions

The availability of always larger datasets of high-frequency price series and the application of computer-intensive methods for analyzing their properties have opened new horizons to researchers in finance and have emphasized the need to develop alternative modeling paradigms. The statistical analyses of price variations in financial markets, such as the stock market, reveal important statistical properties of the asset returns such as distributional properties, tail properties and extreme fluctuations, pathwise regularity, linear and nonlinear dependence of returns in time and across stocks. These statistical properties invalidate many of the mainstream asset pricing models and open the way to behavioral finance, specifically to asset pricing models with heterogeneous and interacting traders. These models try to provide a behavioral explanation for this set of properties that are common across many financial instruments, markets and time periods and are classified as

stylized facts. These financial models have a deterministic skeleton represented by nonlinear (often piecewise smooth, or piecewise continuous) dynamical systems that deserve a mathematical investigation.

The current contribution goes in this direction and our goal in this work has been twofold. First, we have developed a new model, which generalizes previous studies performed with one-dimensional discontinuous systems, showing that a two-dimensional extension leads to dynamics which are better related to real markets. Second, new analytical results are derived that explicitly give the border collision bifurcations conditions related to basic cycles, which are the starting tools in the period adding bifurcation structure. These analytical results are employed to insight on the economic mechanisms behind time series of asset returns that are consistent with empirical data.

The current work belongs to the realm of economic and financial applications of piecewise linear maps and can be extended in different directions. Regarding the deterministic dynamics, we have only partially analyzed some regimes in terms of the possible values of the parameters. Several different cases are also interesting in the applied context, both with regular and chaotic dynamics, which are left for future studies, and clearly the related perturbed system may also be relevant in the application here considered. Concerning, instead, the modeling and normative aspects, to arouse recently particular interest are the applications devoted to study the effects of regulations or policy interventions aimed to stabilize the financial markets. The policy interventions are based on taxes or trading limitation mechanisms that impact on the smoothness of the asset pricing models, see, e.g., Anufriev and Tuinstra [1], in 't Veld [49] and Dercole and Radi [14]. An extension of our setup to study possible form of regulations represents an interesting contribution. The relatively simple deterministic structure of our setup justifies an attempt to provide an empirical validation of the proposed model. In this direction, we mention Boswijk et al. [8], Hommes and in 't Veld [28] and Schmitt [39]. The use of experiments to validate our setup is another relevant and possible future work to put in the research agenda.

Acknowledgements Work developed in the framework of the research project on *Models of behavioral economics for sustainable development* of the Department of Economics, Society, Politics (DESP), University of Urbino. Davide Radi acknowledges the support of the Czech Science Foundation (GACR) under project [20-16701S] and VSB-TU Ostrava under the SGS project SP2020/11.

Compliance with Ethical Standards

Conflicts of interest The authors declare that they have no conflict of interest.

References

1. Anufriev, M., Tuinstra, J.: The impact of short-selling constraints on financial market stability in a heterogeneous agents model. J. Econ. Dyn. Control **37**(8), 1523–1543 (2013)
2. Avrutin, V., Schanz, M., Banerjee, S.: Multi-parametric bifurcations in a piecewise-linear discontinuous map. Nonlinearity **19**(8), 1875–1906 (2006)
3. Avrutin, V., Zhusubaliyev, Z., Saha, A., Banerjee, S., Sushko, I., Gardini, L.: Dangerous bifurcations revisited. Int. J. Bifurc. Chaos **26**(14), 1630040 (2016)
4. Avrutin, V., Gardini, L., Sushko, I., Tramontana, F.: Continuous and Discontinuous Piecewise-Smooth One-Dimensional Maps. World Scientific Series on Nonlinear Science A, vol. 95. World Scientific, Singapore (2019)
5. Banerjee, S., Yorke, J.A., Grebogi, C.: Robust chaos. Phys. Rev. Lett. **80**(14), 3049–3052 (1998)
6. Beja, A., Goldman, M.B.: On the dynamic behavior of prices in disequilibrium. J. Finance **35**(2), 235–248 (1980)
7. Blaurock, I., Schmitt, N., Westerhoff, F.: Market entry waves and volatility outbursts in stock markets. J. Econ. Behav. Organ. **153**, 19–37 (2018)
8. Boswijk, H.P., Hommes, C.H., Manzan, S.: Behavioral heterogeneity in stock prices. J. Econ. Dyn. Control **31**(6), 1938–1970 (2007)
9. Brianzoni, S., Campisi, G.: Dynamical analysis of a financial market with fundamentalists, chartists, and imitators. Chaos Solitons Fractals **130**(109), 434 (2020)
10. Brock, W.A., Hommes, C.H.: Heterogeneous beliefs and routes to chaos in a simple asset pricing model. J. Econ. Dyn. Control **22**, 1235–1274 (1998)
11. Chiarella, C., Dieci, R., He, X.Z.: Handbook of Financial Markets: Dynamics and Evolution, North-Holland, chap Chapter 5 - Heterogeneity, Market Mechanisms, and Asset Price Dynamics, pp. 277–344 (2009)
12. Cont, R.: Empirical properties of asset returns: stylized facts and statistical issues. Quant. Financ. **1**(2), 223–236 (2001)
13. Day, R.H., Huang, W.: Bulls, bears and market sheep. J. Econ. Behav. Organ. **14**(3), 299–329 (1990)
14. Dercole, F., Radi, D.: Does the "uptick rule" stabilize the stock market? insights from adaptive rational equilibrium dynamics. Chaos Solitons Fractals **130**(109), 426 (2020)
15. di Bernardo, M., Budd, C.J., Champneys, A.R., Kowalczyk, P.: Piecewise-Smooth Dynamical Systems: Theory and Applications. Applied Mathematical Sciences, vol. 163. Springer, London (2008)
16. Dieci, R., Schmitt, N., Westerhoff, F.: Steady states, stability and bifurcations in multi-asset market models. Decis. Econ. Financ. **41**(2), 357–378 (2018)

17. Do, Y., Kim, S., Kim, P.: Stability of fixed points placed on the border in the piecewise linear systems. Chaos Solitons Fractals **38**(2), 391–399 (2008)
18. Dutta, P.S., Banerjee, S.: Period increment cascades in a discontinuous map with square-root singularity. Discret. Contin. Dyn. Syst. Ser. B **14**(3), 961–976 (2010)
19. Dutta, P.S., Routroy, B., Banerjee, S., Alam, S.S.: On the existence of low-period orbits in n-dimensional piecewise linear discontinuous maps. Nonlinear Dyn. **53**(4), 369–380 (2008)
20. Farmer, J.D., Joshi, S.: The price dynamics of common trading strategies. J. Econ. Behav. Organ. **49**(2), 149–171 (2002)
21. Garcia-Morato, L.B., Macias, E., nez, E.N., Peral, F.: Bifurcation patterns in homogeneous area-preserving piecewise-linear maps. Qual. Theory Dyn. Syst. **18**(2), 547–582 (2019)
22. Gardini, L., Tramontana, F., Avrutin, V., Schanz, M.: Border collision bifurcations in $1d$ pwl map and Leonov's approach. Int. J. Bifurc. Chaos **20**(10), 3085–3104 (2010)
23. Gaunersdorfer, A., Hommes, C.H., OOWagener, F.: Bifurcation routes to volatility clustering under evolutionary learning. J. Econ. Behav. Organ. **67**(1), 27–47 (2008)
24. Gu, E.G.: Bifurcations and chaos for 2D discontinuous dynamical model of financial markets. Int. J. Bifurc. Chaos **27**(12), 1750185 (2017)
25. Gu, E.G.: On the existence of chaos in a discontinuous area-preserving map arising in financial markets. Int. J. Bifurc. Chaos **28**(14), 1850177 (2018)
26. He, X.Z., Li, Y.: Heterogeneity, convergence, and autocorrelations. Quant. Financ. **8**(1), 59–79 (2008)
27. Hofbauer, J., Sigmund, K.: Evolutionary game dynamics. Bull. (New Series) Am. Math. Soc. **40**(4), 479–519 (2003)
28. Hommes, C., Veld, D.: Booms, busts and behavioural heterogeneity in stock prices. J. Econ. Dyn. Control **80**, 101–124 (2017)
29. Kollár, L.E., Stépán, G., Turi, J.: Dynamics of piecewise linear discontinuous maps. Int. J. Bifurc. Chaos **14**(7), 2341–2351 (2004)
30. Lu, S., Oberst, S., Zhang, G., Luo, Z.: Bifurcation analysis of dynamic pricing processes with nonlinear external reference effects. Commun. Nonlinear Sci. Numer. Simul. **79**(104), 929 (2019)
31. Lux, T.: The socio-economic dynamics of speculative markets: interacting agents, chaos, and the fat tails of return distributions. J. Econ. Behav. Organ. **33**(2), 143–165 (1998)
32. Lux, T., Ausloos, M.: The Science of Disasters. Market Fluctuations I: Scaling, Multiscaling, and Their Possible Origins, pp. 372–409. Springer, New York (2002)
33. Lux, T., Marchesi, M.: Scaling and criticality in a stochastic multi-agent model of a financial market. Nature **397**, 498–500 (1999)
34. Mira, C.: Global Analysis of Dynamic Models for Economics, Finance and Social Sciences. Embedding of a Dim1 Piecewise Continuous and Linear Leonov Map into a Dim2 Invertible Map, pp. 337–368. Springer, New York (2013)
35. Mira, C., Gardini, L., Barugola, A., Cathala, J.C.: Chaotic Dynamics in Two-dimensional Noninvertible Maps. World Scientific Series on Nonlinear Science A, vol. 20. World Scientific, Singapore (1996)
36. Nusse, H.E., Yorke, J.A.: Border-collision bifurcations including "period two to period three" for piecewise smooth systems. Phys. D **57**(1–2), 39–57 (1992)
37. Nusse, H.E., Yorke, J.A.: Border-collision bifurcations for piecewise smooth one-dimensional maps. Int. J. Bifurc. Chaos Appl. Sci. Eng. **5**(1), 189–207 (1995)
38. Rakshit, B., Apratim, M., Banerjee, S.: Bifurcation phenomena in two-dimensional piecewise smooth discontinuous maps. Chaos Interdiscip. J. Nonlinear Sci. **20**, 033101 (2010)
39. Schmitt, N.: Heterogeneous expectations and asset price dynamics, Bamberg Economic Research Group (BERG) Working Paper Series, No. 134 (2018)
40. Simpson, D.: Bifurcations in Piecewise-Smooth Continuous Systems. World Scientific, Singapore (2010)
41. Simpson, D.: Sequences of periodic solutions and infinitely many coexisting attractors in the border-collision normal form. Int. J. Bifurc. Chaos **24**(6), 1430018 (2014)
42. Simpson, D.: The stability of fixed points on switching manifolds of piecewise-smooth continuous maps. arXiv:1612.02932v1 (2016)
43. Simpson, D.: Unfolding codimension-two subsumed homoclinic connections in two-dimensional piecewise-linear maps. arXiv:1907.02653v1 (2019)
44. Simpson, D., Tuffley, C.: Subsumed homoclinic connections and infinitely many coexisting attractors in piecewise-linear continuous maps. Int. J. Bifurc. Chaos **27**(2), 1730010 (2017)
45. Sushko, I., Gardini, L.: Center bifurcation for two-dimensional border collision normal form. Int. J. Bifurc. Chaos **18**(4), 1029–1050 (2008)
46. Sushko, I., Gardini, L.: Degenerate bifurcations and border collisions in piecewise smooth 1d and 2d maps. Int. J. Bifurc. Chaos **20**(7), 2045–2070 (2010)
47. Tramontana, F., Westerhoff, F., Gardini, L.: On the complicated price dynamics of a simple one-dimensional discontinuous financial market model with heterogeneous interacting traders. J. Econ. Behav. Organ. **74**(3), 187–205 (2010)
48. Tramontana, F., Gardini, L., Westerhoff, F.: A simple financial market model with chartists and fundamentalists: market entry levels and discontinuities. Math. Comput. Simul. **108**, 16–40 (2015)
49. Veld, D.: Adverse effects of leverage and short-selling constraints in a financial market model with heterogeneous agents. J. Econ. Dyn. Control **69**, 45–67 (2016)
50. Zhusubaliyev, Z., Mosekilde, E.: Bifurcations and Chaos in Piecewise-Smooth Dynamical Systems. World Scientific Series on Nonlinear Science A, vol. 44. World Scientific, Singapore (2003)